OULU 2018
C 669

ACTA UNIVERSITATIS OULUENSIS

Severi Anttila

INFLUENCE OF MINOR ELEMENTS ON SOME WELDABILITY ISSUES OF INTERMEDIATE PURITY STABILIZED FERRITIC STAINLESS STEELS

UNIVERSITY OF OULU GRADUATE SCHOOL;
UNIVERSITY OF OULU,
FACULTY OF TECHNOLOGY

ACTA UNIVERSITATIS OULUENSIS
C Technica 669

SEVERI ANTTILA

INFLUENCE OF MINOR ELEMENTS ON SOME WELDABILITY ISSUES OF INTERMEDIATE PURITY STABILIZED FERRITIC STAINLESS STEELS

Academic dissertation to be presented with the assent of the Doctoral Training Committee of Technology and Natural Sciences of the University of Oulu for public defence in the Arina auditorium (TA105), Linnanmaa, on 7 September 2018, at 12 noon

UNIVERSITY OF OULU, OULU 2018

Copyright © 2018
Acta Univ. Oul. C 669, 2018

Supervised by
Professor David Porter

Reviewed by
Professor John Lippold
Professor Lars-Erik Svensson

Opponent
Professor Veli Kujanpää

ISBN 978-952-62-1972-1 (Paperback)
ISBN 978-952-62-1973-8 (PDF)

ISSN 0355-3213 (Printed)
ISSN 1796-2226 (Online)

Cover Design
Raimo Ahonen

JUVENES PRINT
TAMPERE 2018

Anttila, Severi, Influence of minor elements on some weldability issues of intermediate purity stabilized ferritic stainless steels.
University of Oulu Graduate School; University of Oulu, Faculty of Technology
Acta Univ. Oul. C 669, 2018
University of Oulu, P.O. Box 8000, FI-90014 University of Oulu, Finland

Abstract

Stabilized ferritic stainless steel grades are attractive alternatives to common austenitic grades in sheet metal applications. Compared with older unstabilized ferritic grades, the mechanical and corrosion properties are usually improved. The impurity level, mainly the amount of interstitial carbon and nitrogen, plays an important role in these steels. There are notable issues in the welding of these steels, the most apparent difference to austenitic steels is the susceptibility to brittle failure. This research focused on the influence of minor elements, especially aluminium, calcium, silicon, titanium, niobium, nitrogen and oxygen, on the weldability of modern intermediate purity level stabilized ferritic stainless steels. The research proceeded in several stages. At first, the general characteristics and performance data about the welds in currently manufactured 11 to 21 mass percent chromium ferritic stainless steels in Europe was obtained. The research then focused on novel high chromium stabilized ferritic stainless steels. Lastly, the influence of various steelmaking practices on weldability were investigated.

The results showed that in stabilized ferritic stainless steels, slag islands are frequently seen in the molten weld pools. These islands can have many origins, e.g. deoxidation, calcium treatment and stabilization practices, and they can be roughly assessed from the chemical composition of the steel. The nature and the influence of these slags varies and can be related to irregularities in the weldability and molten metal fluid flow.

Large grain size and titanium carbonitride particles impair the toughness of the heat-affected zone. Generally, stabilization with niobium is preferred. However, solely niobium stabilized steel welds run the risk of forming coarse columnar grains in welds deteriorating some of the properties. A breakdown of the columnar grains is possible to achieve in autogenous welds with minor titanium and aluminium alloying, provided that small amounts of nitrogen and oxygen are induced from the shielding gas. However, grain refinement may not improve the properties, if it is accomplished with an increase in the total interstitial content.

Keywords: alloying, corrosion resistance, ductility, ferritic stainless steel, grain refinement, slag islands, toughness, welding

Anttila, Severi, Ferriittisten ruostumattomien terästen hitsattavuuden ongelmakohtia keskipuhtailla stabiloiduilla teräslajeilla.
Oulun yliopiston tutkijakoulu; Oulun yliopisto, Teknillinen tiedekunta
Acta Univ. Oul. C 669, 2018
Oulun yliopisto, PL 8000, 90014 Oulun yliopisto

Tiivistelmä

Stabiloidut ferriittiset ruostumattomat teräkset soveltuvat korvaamaan tavanomaisia austeniittisia ruostumattomia teräksiä ohutlevysovelluksissa. Näillä teräksillä keskeiset mekaaniset ja korroosio-ominaisuudet ovat usein paremmat kuin varhaisilla, stabiloimattomilla ferriittisillä teräksillä. Hiili ja typpi ovat näissä teräksissä kuitenkin epäpuhtauksia. Toisin kuin austeniittiset teräkset, ferriittiset teräkset ovat alttiita haurasmurtumalle, erityisesti hitsatuissa rakenteissa. Tässä väitöstutkimuksessa keskityttiin mikroseosaineiden ja epäpuhtauksien vaikutukseen keskipuhtaiden stabiloitujen ferriittisten teräslajien hitsauksessa. Tutkimus kohdistui erityisesti alumiinin, kalsiumin, piin, titaanin, niobin, typen ja hapen vaikutuksiin. Aluksi tutkittiin kaupallisten terästen hitsien keskeisiä ominaisuuksia. Tämän jälkeen tutkittiin uusia ns. korkeakromisia stabiloituja ferriittisiä teräslajeja. Lopuksi tutkittiin teräksen valmistuksen vaikutuksia stabiloitujen ferriittisten ruostumattomien terästen hitsattavuuteen.

Tutkituilla teräksillä hitsauksen aikana muodostui runsaasti kuonalauttoja. Näillä kuonilla on monta alkuperää, esim. deoksidointi, kalsiumkäsittely ja stabilointiaineet. Hitsien kuonaisuutta voidaan karkeasti arvioida teräksen kemiallisen koostumuksen perusteella. Muodostuvilla kuonilla on useita vaikutuksia hitsauksessa, mm. epäjatkuvuuksiin ja sulan virtauksiin.

Hitsauksessa muodostuva suuri raekoko ja stabiloinnin titaanikarbonitridipartikkelit heikentävät oleellisesti hitsin muutosvyöhykkeen sitkeyttä. Stabilointi käyttäen pääasiassa niobia on toivottavaa, mutta jos stabilointiin käytetään vain niobia, tulee hitsin mikrorakenteesta karkea ja hitsin ominaisuudet voivat heikentyä. Karkean mikrorakenteen hienontaminen on mahdollista käyttäen suojakaasuna argonia, jossa on hieman typpeä ja happea, mikäli teräkseen on seostettu hieman alumiinia ja titaania. Raerakenteen hienontaminen ei kuitenkaan yksiselitteisesti paranna hitsin ominaisuuksia, mikäli hienontaminen saavutetaan kasvattamalla epäpuhtauspitoisuutta tarpeettoman korkeaksi.

Asiasanat: ferriittinen ruostumaton teräs, hitsaus, korroosio, kuonalautat, raekoon hienontaminen, seosaineet, sitkeys

Acknowledgements

The work presented in this thesis was carried out during the years 2010–2017 in various projects dealing with the welding of ferritic stainless steels. The research work started in the project “Structural Applications of Ferritic Stainless Steels” (SAFSS) funded by the European Community's Research Fund for Coal and Steel (RFCS), in which the basic properties of welds in various commercial 11–21 wt.% Cr ferritic stainless steels were examined. After the RFCS project, the weldability of novel 21 wt.% Cr stabilized ferritic stainless steel grades were investigated in the New Generation Ferritic Stainless Steels (NGF) of Demanding Applications programme of Finnish Metals and Engineering Competence Cluster (FIMECC). The concluding research focused on the effects of various melt shop practices of the welding properties of stabilized ferritic stainless steels. This work has been carried out during the Breakthrough Steels and Applications (BSA) programme of the Digital, Internet, Materials & Engineering Co-Creation (DIMECC).

The work received funding from the RFCS Grant Agreement No. RFSR-CT-2010-00026, Technology Industries of Finland Centennial Foundation Fund for the Association of Finnish Steel and Metal Producers (Metallinjalostajien rahasto), Advanced Materials Doctoral Programme (ADMA-DP) of the University of Oulu Graduate School, Tauno Tönningin säätiö, Jenny and Antti Wihuri Foundation and the University of Oulu Scholarship Foundation. I am grateful for all of the support.

During this time, I have received guidance and support from various experts and I am very grateful for their help. I would especially like to thank my supervisor Professor David Porter, Professor Emeritus Pentti Karjalainen, Professor Jukka Kömi, Professor Timo Fabritius and Dr. Jouko Leinonen for their valuable guidance and comments over the course of this work.

Furthermore, a major part of the work was carried out at Outokumpu Stainless Oy, Tornio Research Centre. The support and guidance received from Dr. Mikko Ylitalo, Mr. Jukka Säynäjäkangas and Dr. Leeni Aula are appreciated.

In addition, I am also thankful to several researchers, technicians and others who helped me during the thesis process. Special thanks to Mr. Tuomas Alatarvas, Dr. Matti Aula, Dr. Eetu-Pekka Heikkinen, Mr. Hannu-Pekka Heikkinen, Mr. Seppo Lantto, Mr. Vesa Lauhikari and Mr. Juha Uusitalo.

Finally, I would like to thank my family and friends for their support during these years.

Oulu, October 2017 Severi Anttila

Symbols and abbreviations

$\Delta t_{8/5}$	Cooling time from 800 to 500 °C [s]
R^2	Coefficient of determination
R^2(adj.)	Coefficient of determination adjusted for the number of predictors
AOD	Argon oxygen decarburization
ASTM	Steel grade in ASTM specifications
CCD	Charge-coupled device
C_V	Absorbed energy [J/cm^2]
$C_{V\text{-}US}$	Upper shelf energy [J/cm^2]
DBTT	Ductile-brittle transition temperature, 35 J/cm^2 [°C]
DCEN	Direct current electrode negative
D/W	Weld depth-to-width ratio
EBM	Electron beam melting
EBSD	Electron backscatter diffraction
ECD	Equivalent circle diameter
EDS	Energy-dispersive X-ray spectrometer
EN	Steel grade in the Euronorm
ER	Preface to a filler metal electrode classification
FF	Kaltenhauser ferrite factor
GMA	Gas metal arc
GS	Average grain size, mean linear intercept [µm]
GTA	Gas tungsten arc
HAZ	Weld heat-affected zone
HTE	High-temperature embrittlement
HTHAZ	High-temperature weld heat-affected zone
HV	Vicker's hardness
LOM	Light optical microscope
LCF	Laser confocal microscope
m	Fitting constant
PRE	Pitting resistance equivalent number
PWHT	Post weld heat treatment
SA	Fraction of ductile fracture in a fractured Charpy-V specimen [%]
SE	Standard error
SEM	Scanning electron microscope
SMA	Shielded metal arc
STEM	Scanning transmission electron microscope

UNS	Steel grade in Unified Numbering System
USE	Upper shelf energy [J/cm^2]
VIM	Vacuum induction melting
VIF	Variance inflation factor
VOD	Vacuum oxygen decarburization
W_b/W_f	Weld root bead width to weld face width ratio
YAG	Yttrium aluminium garnet

List of original publications

This thesis is based on the following publications, which are referred throughout the text by their Roman numerals:

I Anttila S, Lauhikari V, Heikkinen H-P & Porter D (2016) Slag island characteristics and weld penetration in very low sulphur 18% Cr stabilized ferritic stainless steel, Welding in the World 60(3): 485–496.

II Anttila S, Aula M & Porter D (2017) Behaviour and influence of slag islands in ferritic stainless steel welds, Welding in the World 61(6): 1141–1154

III Anttila S, Karjalainen P & Lantto S (2013) Mechanical properties of ferritic stainless steel welds in using type 409 and 430 filler metals, Welding in the World 57(3): 335–347.

IV Anttila S, Heikkinen H-P, Säynäjäkangas J & Porter D (2015) Impact energy and fracture appearance in welds of some ferritic stainless steels, Proc 8th European Stainless Steel Conference, Austrian Society for Metallurgy and Materials (ASMET).

V Anttila S, Alatarvas T & Porter D (2017) Factors affecting impact toughness in stabilized intermediate purity 21Cr ferritic stainless steels and their simulated heat-affected zones, Metallurgical and Materials Transactions A 48(12): 5879–5889.

VI Anttila S & Porter D (2014) Influence of shielding gases on grain refinement in welds of stabilized 21%Cr ferritic stainless steel, Welding in the World 58(6): 805–817.

The author has been the main and corresponding author of all above publications. The author planned the tests, performed the experiments and data analyses, excluding the analysis of spectroscopy in Paper II, practical welding experiments in Paper III, Gleeble simulations in Papers IV–V, some tensile tests and impact toughness tests for Paper IV, electrolytic extraction for Paper V, some scanning electron microscopy and transmission electron microscopy for Paper V and high temperature tensile tests for Paper VI. David Porter has commented on all papers, and Pentti Karjalainen on Paper III.

In Paper I, the influence of the chemical composition and welding parameters on slag island formation and the level of penetration is examined in 31 commercial intermediate purity stabilized ferritic stainless steel heats. The key characteristics are investigated and regression models are prepared to understand how the tendency of slagging and penetration vary between steels due to minor elements. Paper II continues the research into further details and introduces *in situ* assessments into the slagging phenomenon via weld pool imaging, spectroscopy and welding parameter monitoring.

Paper III is a comprehensive study about the mechanical properties of ferritic stainless steel welds fabricated using ferritic filler metals in commercial

intermediate purity ferritic stainless steels. This work presents the key results of the author's master's thesis "Mechanical and Corrosion Properties of Ferritic Stainless Steels Welded with Ferritic Filler Metals" with some additional testing.

Paper IV investigates the correlation between fracture appearance and impact toughness in ferritic stainless steel base metals, heat-affected zones and weld metals in 17 commercial steels. Furthermore, Paper V clarifies how minor elements originating from the stabilization affect impact toughness in intermediate purity high Cr ferritic stainless laboratory steels and their simulated heat-affected zones.

Paper VI describes an experimental investigation about the influence of shielding gases on the grain refinement in high Cr ferritic stainless commercial and laboratory steels. The results of this paper have previously been presented in the author's licentiate thesis "Properties of Welds in 21%Cr Ferritic Stainless Steels".

Table of contents

1 Introduction

1.1 Background

The stainless steel industry in Europe is rediscovering itself, as seen from reorganization and merging of large companies. Limited growth possibilities in Europe and increasing raw-material costs are damaging the profitability of the industry. Now, steel producers and customers are finding out that cost-stability is an increasingly preferred property in stainless steel. Ordinary austenitic stainless steels are subject to price-changes due to the fluctuations of Ni and Mo in metal markets. Therefore, Ni-free steel grades such as those of ferritic stainless steels offer viable alternatives for many applications requiring sufficient or comparable corrosion resistance [1–3].

Ferritic stainless steel grades were prevalent in the 1950s during the Ni-shortage era of the Korean War [1, 4]. Since then, a resurrection of interest in ferritic grades has frequently occurred when the supply of Ni has been restricted or its market price skyrocketed. According to the International Stainless Steel Forum, the market share of ferritic and martensitic grades (i.e., the 400 series) in the year 2016 was around 23% worldwide [5]. Approximately half of the ferritic stainless steels are still traditional *unstabilized* grades, but there has been a tendency for *stabilized* grades to become more popular.

The majority of developments and research into ferritic stainless steel grades and their weldability was done in the 1970s, when new melting practises made it possible to commercially produce steels with intermediate and low interstitial contents. Within the next decades, the focus was on low Cr utility grades that were introduced in the late 1980s [1]. In the 2000s, the development and commercial attention has been on intermediate and low interstitial high Cr range (20–24%Cr) [6–11]. This Cr range has been somewhat vacant even though ultra-pure superferritic grades (>26%Cr) have existed since the development of refining techniques in the 1970s.

Constitution of ferritic stainless steel grades is different from those of austenitic grades. Ferritic grades cannot bear interstitial C and N similar to those of austenitic grades without having corrosion issues, particularly after welding [12–14]. This is due to Cr carbide and nitride precipitation that occurs very rapidly in ferrite due to low solubility of interstitials at high temperatures. Therefore, many modern ferritic grades are alloyed with so-called stabilizing elements such as Ti and Nb. This

stabilization improves the corrosion resistance by preventing Cr-based precipitation that could lead to intergranular corrosion. Interstitial contents similar to those of austenitic grades are also detrimental to the toughness of ferritic stainless steels and to prevent brittle failure in service, these materials are usually supplied in sheet form [15–17].

The manufacturing process of ferritic grades is different from those of typical austenitic grades. The deoxidation process, which is compulsory for stainless steel manufacturing, is typically accomplished with Al, FeSi and Mn. When using stabilizing elements, the precipitation or secondary particles often begins in molten metal. For example, very stable Ti nitrides can already be present in the molten state in continuous casting. These nitrides tend to accumulate with the oxide particles from deoxidation and cause severe nozzle clogging problems in casting, restricting the production process. A well-known solution to prevent this phenomenon is to lower the melting point of deoxidation products such as Al oxides via alloying trace amounts of Ca to the steel, i.e., calcium treatment. Consequently, the high-melting-point Al oxides are substituted with low-melting-point calcium aluminates. These low-melting-point substrates can prevent the nitride accumulation in casting and alleviate nozzle clogging. Therefore, the productivity of stabilized ferritic grades is significantly improved.

1.2 Aims of the research

Even though weldability, i.e., ability to produce sound welds with satisfactory mechanical and corrosion properties, of ferritic stainless steels has been researched somewhat plentifully over the last 40 years, some areas have not received much attention. The welding research into new stabilized high-Cr (20–24%Cr) alloys has not been sufficient due to their relatively recent developments. There is also an apparent lack of research about the weldability issues in calcium-treated intermediate purity stabilized ferritic stainless steels. Moreover, information published about welded joints fabricated with ferritic filler metals has been lacking. Therefore, this thesis aims to address some of the needed research into the following topics:

- To study how significant of an effect minor elements typically seen on modern intermediate purity stabilized ferritic steels have on weld properties
- To clarify how trace amounts of Ca influence weldability

- To study the influence of the weld metal microstructure on mechanical and corrosion properties
- To study how heat input influences the precipitate and inclusion size, type, distribution and grain size, and how these affect toughness
- To clarify how the method of stabilization influences microstructure and properties at intermediate interstitial levels

Information gathered from these topics will result in up-to-date knowledge regarding the weldability of modern intermediate purity stabilized ferritic stainless steels. This research aims to summarize how the weldability of these materials is influenced by minor elements originating from the stabilization, deoxidation, desulphurization and calcium treatment, and how potential welding issues can be mitigated. Lastly, although having marginal scientific novelty, the benchmarking data provides practical knowledge about the position of welded stabilized intermediate purity ferritic stainless steels in the field of other ferritic stainless steel grades.

2 Theoretical foundation

2.1 Engineering properties, alloying and limitations

Ferritic stainless steels are Fe-Cr-based alloys that are rarely alloyed with high amounts of austenite-forming substitutional elements such as Ni, Mn, Cu or Co. Owing to high Cr concentration and low austenite potential, the cubic crystal structure in these steels remains predominantly body-centred cubic to the solidus temperature, although martensite in various amounts may exist in the microstructure of some grades.

The main advantage of ferritic grades is their cost stability in comparison with Ni-bearing austenitic grades, but there are also other properties that separate the two steel groups. Ferritic grades have a superior resistance to chloride-induced stress corrosion cracking, are resistant to corrosion by reducing acids and have improved deep-drawability and machinability, higher yield strength and a lower thermal expansion coefficient in comparison with austenitic grades [1, 3, 18, 19]. The major disadvantages are notch-sensitivity and subsequent limited toughness in the base metals and welds, grade-dependent weldability, low work hardening and various second phase embrittlement phenomena that may occur when heat treated [4, 13, 20–26].

Ferritic grades cover a wide range of corrosion and heat-resisting alloys, from low-cost 10–14 wt.% Cr grades to superferritic grades that contain 25–30 wt.% Cr and also some Mo and Ni [3, 27]. As corrosion resistance is mainly determined by the amount of Cr, the differences in corrosion performance within different grades can be vast. The low-Cr grades do not retain their stainless appearance for very long, as pitting corrosion and staining can occur even in ordinary dry atmospheric conditions. The medium-Cr grades have greater tolerance against staining, but applications are typically limited to dry indoor use. The high-Cr grades have much greater tolerance against corrosion phenomena, and the *pièce de résistance*, the superferritics, can be used in very demanding applications, requiring exposure to high-chloride seawater. Some applications for ferritic grades are coal wagons, shipping containers, bus frames and panels, automotive exhaust systems, household utensils, indoor decorative panels, kitchen sinks, water piping, automotive trim, outdoor panels, boilers and heat transfer in nuclear condenser and seawater exchanger tubing [3].

An important metallurgical feature in understanding ferritic grades is the interstitial content, mainly the sum of C and N, that are considered impurities in these steels [22]. Extensive precipitation of carbides, nitrides and carbonitrides, or even transformation to austenite and subsequently to martensite is not uncommon [28, 29]. Of these, the most detrimental in heat treatments are the readily forming Cr-based precipitates that can deplete the Cr concentration near the particles and cause *sensitization*, typically at grain boundaries. These sensitized regions experience rapid corrosion rates as the protective Cr oxide film may have become damaged [22, 30]. To prevent this, the stabilized ferritic grades are alloyed with stable carbide and nitride-forming elements such as Ti, Nb, Ta, Zr and V. This is especially important for steels intended for welding, because otherwise, costly post weld heat treatments (PWHTs) may be required to restore the corrosion protection in the welded area [13].

2.1.1 Developments in ferritic stainless steel grades

Over the course of about the last 100 years, many basic ferritic stainless steel grades have evolved from their historical beginnings. New refining techniques that became common in the 1970s were quickly adopted and made it possible to manufacture ferritic grades with low interstitial contents on a commercial scale [1, 19, 31]. Argon oxygen decarburization (AOD) produced an intermediate interstitial purity level of 200–500 mass ppm, whereas electron beam melting (EBM), vacuum induction melting (VIM) and vacuum oxygen decarburization (VOD) made it possible to manufacture grades that contained very low amounts of interstitials, frequently below 100 ppm [31, 32]. Table 1 lists a selection from the most recent EN 10088-1:2014 ferritic corrosion resisting steel alloys with some key alloying elements and comparative equations with respect to their phase balance and corrosion resistance.

Table 1. Some ferritic stainless steel alloys from EN 10088-1:2014 [11] (wt.%).

EN	UNS/ASTM	C	N	Cr	Mo	Others	FF[2]	PRE[3]
Low Cr grades								
1.4003	S40977	≤0.03	≤0.03	10.5–12.5	–	–	7–8	11–13
1.4512	409	≤0.03	–	10.5–12.5	–	Ti[1]	11–14	11–13
Medium Cr grades								
1.4016	430	≤0.08	–	16–18	–	–	12–16	16–18
1.4510	439	≤0.05	–	16–18	–	Ti[1]	18–21	16–18
1.4509	S43940	≤0.03	–	17.5–18.5	–	Ti, Nb	20–23	18–19
1.4521	444	≤0.025	≤0.03	17–20	1.8–2.5	Ti[1]	28–31	23–28
High Cr grades								
1.4611	–	≤0.03	–	19–22	≤0.5	Ti[1], Ni, Cu	21–24	20–24
1.4621	445	≤0.03	≤0.03	20–21.5	–	Nb, Cu	21–23	20–22
1.4613	–	≤0.03	–	22–25	≤0.5	Ti[1], Ni, Cu	22–26	23–26
1.4592	S44735	≤0.025	≤0.045	28–30	3.5–4.5	Ti[1]	> 40	40–45

[1] stabilization also permitted with Nb and Zr,

[2] FF = Kaltenhauser ferrite factor = Cr + 6Si + 8Ti + 4Mo + 2Al – 40(C+N) – 2Mn – 4Ni [18],

[3] PRE = pitting resistance equivalent = Cr + 3.3Mo + 16N

The Kaltenhauser ferrite factor (FF) shown in the table is a rough estimate of the phase balance after welding: values below 8 indicate a predominantly martensitic microstructure, values between 8 and 13.5 propose dual-phased ferritic-martensitic microstructure, and values greater than 13.5 fully ferritic. The pitting resistance equivalent (PRE) number approximates the corrosion resistance of an alloy, i.e., the higher the value, the greater the resistance to corrosion. Obviously, a wide variety of ferrite potential can be established with different grades, and corrosion resistance increases with higher alloyed grades.

The workhorse of ferritic stainless steel grades has been 1.4016 (ASTM type 430), which is one of the oldest stainless steels on the market. The early stabilized steel 1.4512 (409) is especially used for automotive exhaust components. Other common stabilized grades originating from the 1970s are 1.4510 (439) and 1.4521 (444). The 1.4509 (S43940, ‘441’) is a relatively recent addition, brought to the EN standard in the 1990s. This steel grade is frequently referred to as ‘441’, as it shares similarities with the type 441 steel grade.

Trend towards high Cr grades

The higher alloyed superferritic steels were engineered as an alternative to Ti, Cu-Ni and superaustenitic alloys for use in seawater and other high-Cl applications

[31, 33, 34]. Compared with other ferritic grades, the superferritics had improved toughness due to the low interstitial content but also superior corrosion resistance in high-Cl and caustic environments [31, 32]. Among the superferritics, three development eras can be distinguished: first, a high-purity era (refining via EBM, ESR, VOD and VIM), then, 2–4 wt.% Ni alloyed era for improved manufacturability and finally, intermediate purity era, where the alloys were produced using AOD, but these alloys had to be stabilized for satisfactory toughness and ductility [32]. Despite the stabilization, the intermediate purity era alloys are typically used as thin sheets (≤ 2 mm) as a result of the brittleness in thicker sections [34]. A medium-Cr Mo-bearing grade corresponding to 1.4521 (444) was developed in the era of superferritics and was originally regarded as one. However, nowadays, this grade is considered to be a general-purpose Mo-bearing grade that has excellent corrosion resistance comparable to that of 1.4401 (316) [35].

As opposed to special-purpose superferritic grades, the other range of high-Cr ferritic alloys is the 20–24 wt.% Cr grades. The notable differences between these and the former are the lower Cr content and absence of abundant Mo and Ni. Thus, these alloys are not intended to compete with the superferritics but to provide cost-stable alternatives to the common austenitic grades 1.4301 (304) and 1.4401 (316) [2, 3]. In addition, these high-Cr grades also provide corrosion and oxidation resistance and high-temperature strength, exceeding those of conventional low- and medium-Cr ferritic grades. The Cr range of 20–24 wt.% has only been explored recently in Europe, i.e., many of the patents have been filed within the last 10 years [36–38]. The standardization of alloys within this Cr range has also started recently, as the high Cr grades listed in Table 1 with PRE values of 20–26 (1.4611, 1.4621, and 1.4613) are all newcomers. These grades contain intermediate to low interstitial contents depending on the refining process and are stabilized. Rather than Ni and Mo alloying, these steels frequently contain 0.3–0.8 wt.% of Cu for improved corrosion resistance in certain environments.

2.1.2 Alloying elements in ferritic stainless steels

Even though 5 wt.% of Cr is enough to produce some Cr enrichment on the surface of a steel, about 10.5 wt.% Cr is required for a sufficiently resilient passive film, and further alloying of Cr provides enhanced corrosion protection and oxidation resistance [39]. Chromium is a weak ferrite former but potent in the amounts

present in stainless steels. The upper limit is about 30 wt.%, because after, that the degree of embrittlement and growth rate of secondary phases accelerates [23, 40].

Molybdenum contributes to the passive layer and to the adjacent transition layer, so that pitting and crevice corrosion resistance improves notably [41–43]. Molybdenum is a potent ferrite former in the amounts alloyed in stainless steels. However, excessive alloying promotes secondary phases, especially sigma and Laves phase embrittlement [13, 44, 45].

Copper improves the general corrosion resistance by suppressing the active dissolution on the surface [46]. It retards the growth of pits, resulting in a lower amount of discoloration [47]. However, in Cl environments, Cu may reduce corrosion resistance, and fine epsilon-Cu precipitation in conjunction with Mo may contribute to stress corrosion cracking [48].

Carbon is an impurity in ferritic stainless steels. Rapid diffusion rates and low solubility of interstitials in ferrite leads to the practically unavoidable formation of carbides. A loss of toughness and ductility is apparent after precipitation [49, 44]. Unlike in austenitic steels, the limitation of C to 0.03 wt.% does not provide immunity to sensitization [19].

Nitrogen behaves similarly to C. The solubility of N in ferrite is limited and the precipitation of various nitrides is usually unavoidable. A significant reduction in toughness and ductility is apparent with high N contents [44, 49]. Unlike in austenitic steels, N in ferritics impairs the corrosion resistance by forming Cr-nitrides, potentially leading to sensitization.

Oxygen is not considered to be detrimental to the toughness of ferritic base metals, despite being an interstitial element and readily forming oxides. Redmond [50] demonstrated that 400 ppm of O did not lead to detrimental toughness in a Nb-stabilized 18 wt.% Cr alloy. Also, Van Zwieten and Bulloch [51] noticed that 650 ppm of O had very little effect on the toughness of the 40 wt.% Cr alloy.

Titanium is used to combine with the interstitials, so that Cr-based precipitation can be avoided. Titanium nitrides and oxides can have a detrimental influence on toughness and surface appearance [50, 52]. Titanium also readily forms sulphide inclusions [53]. When present in solid solution, Ti is a very potent element for solid solution hardening [54]. In welds, Ti alloying generally promotes the formation of equiaxed grains, but excessive alloying reduces ductility [54, 55]. Stabilization with Ti only may impair corrosion performance and promote 475 °C embrittlement [56–59].

Niobium is often used in conjunction with Ti for stabilization. Unlike Ti, Nb combines with the interstitials but does not readily form other inclusions.

Stabilization with Nb generally improves toughness; in solid solution, it is a potent hardener and does not promote surface defects [50]. Also, it has been shown that in partly Nb-stabilized steels, the pitting corrosion potential is higher than with Ti alone [60]. However, excessive Nb alloying promotes interdendritic or grain boundary segregation, which may lead to hot cracking phenomena in the welds and promotes Laves phases [61–64]. Moreover, stabilizing only with Nb frequently leads to distinct formation of coarse columnar grains at the weld centreline [55].

Other stabilizing elements, such as Zr, Ta or V, are rarely used in ferritic stainless steels but can be useful [14, 53, 65]. For example, Nakao et al. [65] showed that Zr alloying can improve weld ductility by preventing Cr-based precipitation and excessive grain coarsening.

Aluminium is usually used as a deoxidizer, but it is also a potent nitride former. Oxidation resistance is also improved with Al alloying [27, 66]. Some have claimed that the high Al content of 0.1–5 wt.% in conjunction with Ti, Cu and several other elements, improves ductility in high interstitial alloys [67, 68].

Silicon is often used in steelmaking as a deoxidizer and also improves the fluidity of the melt. The typical range for Si in ferritic stainless steels is 0.30–0.60 wt.% when modern refining techniques are used. Silicon can also be used for improved oxidation resistance in high-temperature ferritic grades [27]. Some have claimed that 3–5 wt.% Si also provides improvements regarding corrosion resistance in Cr-saving (8 wt.% Cr) steels [69].

Wood [54] describes that to retain a good combination of toughness and ductility, the residual Mn, Si, Ni and Cu contents should be kept at a low level in combination with low interstitial and Ti contents. Nickel alloying can improve toughness, but due to economic reasons, it is usually not utilized in commercial production [70].

2.1.3 Embrittlement phenomena

Secondary phase embrittlement, such as sigma, Laves and 475 °C embrittlement phenomena, can occur in ferritic stainless steels at elevated temperatures. Exposure to certain temperature ranges from several to thousands of hours may be required to form these phases. Highly alloyed ferritic grades are typically more prone to embrittlement, which is why care in design and awareness in use is required when ferritic stainless steels are used at elevated temperatures.

475 °C embrittlement in ferrite occurs in alloys containing over 12 wt.% Cr as a result of the miscibility gap in the Fe-Cr system at 400–550 °C [21]. This is

essentially a very fine precipitation process, clustering of Cr atoms, that occurs in the ferritic matrix [20, 71]. Low-Cr and medium-Cr ferritic alloys are prone to embrittlement after tens to hundreds of hours of exposure, but in high-Cr alloys, it may only take a few hours. The reaction occurs by a nucleation-and-growth mechanism in the 12–24 wt.% Cr range and above this by spinodal decomposition [13]. These, up to 80% Cr-rich clusters are considered to be dislocation blocks along {100} matrix planes, resulting in solid solution hardening and a major reduction in toughness [20, 23]. While the reduction of toughness can occur rapidly, longer exposure also increases hardness and tensile strength. The embrittlement also impairs corrosion resistance because of a depletion of Cr concentration adjacent to Cr-rich clusters. The 475 °C embrittlement phenomenon is reversible as short-term annealing above 550 °C dissolves the clusters.

Sigma-phase intermetallic compounds precipitate at the grain boundaries and are promoted by Cr, Mo and Si [72]. In ferritic stainless steels, the embrittlement is usually associated with high-Cr alloys and a temperature range of 500–900 °C but most readily at 800–850 °C. A significant reduction in toughness, ductility and fatigue resistance can occur due to the embrittlement [13, 22, 73]. If the Mo and Si contents are kept at a low level, the embrittlement is retarded and may require thousands of hours of exposure before occurrence. The sigma phase is also reversible by heating at a range of 900–950 °C for a few hours [74].

Laves phases $(Fe,Cr,Ni)_2(Nb,Mo,Si)$ are seen in a variety of steels, including ferritic stainless steels [25, 75–77]. In stabilized grades, the Fe_2Nb types of particles have been found frequently [78, 79]. Laves phases are said to reduce thermal fatigue, cracking resistance, impact toughness and high temperature strength [63, 80, 81]. However, others have shown that Laves phases can be utilized for creep resistance [82]. A solution annealing as that used for the sigma phase can be used to dissolve Laves phases.

Sensitization to intergranular corrosion can also be categorized as an embrittlement phenomenon. Albeit, initially, it was speculated whether the sensitization mechanism in ferritics is the same as in austenitic steels, it was eventually shown that a similar phenomenon, i.e., Cr carbide and nitride precipitation and subsequent Cr depletion in their vicinity, is responsible for the embrittlement [22, 30]. Short-term heat treatment above 750 °C may not dissolve the Cr precipitates, but it allows Cr diffusion to occur and heal the Cr-depleted regions, thus, restoring the corrosion resistance of the steel.

A high-temperature embrittlement (HTE) phenomenon is typically associated with the welding of unstabilized ferritic grades in regions experiencing peak

temperatures above 1200 °C [12]. When the cooling begins, the matrix quickly becomes supersaturated with respect to the interstitials. This leads to both intergranular and intragranular precipitation. Intragranular precipitation causes solid solution hardening, which reduces the toughness, and intergranular precipitation may lead to sensitization [44, 22].

2.2 Welding of ferritic stainless steels

The weldability of the ferritic stainless steels can be divided into two groups: unstabilized and stabilized steels. The unstabilized steels often undergo complete or partial phase transformation to austenite at high temperatures, subsequently undergoing transformation into martensite during cooling [18]. The stabilized steels usually remain fully ferritic at all temperatures [27].

The weldability of ferritic grades is usually considered good although not as effortless as that of austenitic grades [12, 83, 84]. All modern ferritic grades are weldable with satisfactory results, but there are guidelines to follow to ensure sufficient mechanical and corrosion performance from the joints. Generally, all conventional welding methods can be used to produce sound welds such as gas tungsten arc (GTA), gas metal arc (GMA), shielded metal arc (SMA), plasma arc welding, resistance welding, laser welding and high-frequency welding methods. Submerged arc welding is not preferred because of the high heat input to the workpiece. Welding is normally carried out without preheating or PWHT in sheet thicknesses. In some cases, especially with unstabilized steels, a PWHT may provide improvements to the mechanical and corrosion properties.

2.2.1 Welding guidelines

Ferritic stainless steels are recommended to be welded with minimum heat input, because they are prone to pronounced grain growth in the heat-affected zone (HAZ). Preheating or PWHT is not recommended, so that grain growth and formation of secondary phases can be minimized. In predominantly ferritic steels, the coarse grain size and the formation of martensite impair toughness and ductility [18, 55, 85–87]. Although low-heat-input and high-intensity welding processes are recommended, they may promote sensitization in instances when the high cooling rate hinders precipitation with stabilizing elements at high temperatures, and subsequently, Cr-based precipitation may occur at lower temperatures [88].

The most critical aspect of ferritic stainless steel welds is the retention of adequate toughness [89]. Early medium and high-Cr heat resistant ferritic grades, such as 1.4742 (442) or 1.4762 (446), were particularly brittle after exposure to high temperatures [90–92]. Initially, it was thought that the brittleness was due to the high Cr content and martensite, if present. However, it was later shown that the precipitation of carbides and nitrides caused the toughness to deteriorate [15, 51, 93]. The higher Cr content apparently intensifies precipitation as an adequate weld ductility at the 19 wt.% Cr level is achieved with over 700 ppm of interstitials, but only 80–100 ppm of interstitials are tolerated at the 30 wt.% Cr level [94]. Therefore, to effectively retain the toughness in the welds, any potential sources of impurities and contamination should be eliminated [55]. This is especially the case with high-purity steels, in which vigorous precautions are required to inhibit any pickup [16, 95–97]. According to Deverell [97], most of the problems of the high-purity *E-Brite 26-1* alloy in service were linked to contaminated welds. For example, a clear reduction in toughness was reported when the shielding was insufficient [95].

From a practical standpoint, clean welding equipment, appropriate filler metals, dry basic electrodes or, when possible, an inert shielded process, care in joint preparation and sufficient shielding should be pursued. Abundant shielding with Ar is usually recommended, for both the front and backside of the weld [31]. For example, in GTA welding of high-purity steels, large gas cups should be used with a gas lens apparatus [98]. Helium can be used to improve weld penetration and productivity. Hydrogen, nitrogen or oxygen additions should be avoided, since hydrogen may cause hydrogen-induced cracking, nitrogen may cause a decrease in toughness and corrosion resistance, and oxygen may cause porosity. However, in GMA welding, the use of 1–3 vol.% O_2 or CO_2 in Ar-based shielding is preferred to stabilize the arc. Welding defects, such as undercutting or poor penetration, should be avoided because of notch sensitivity [31]. Sharp notches or fatigue cracks in welds are detrimental to toughness [24].

Austenitic filler metals are usually preferred because of their availability and because they provide improved weld metal ductility and toughness; however, the filler metal should have corrosion performance that is at least comparable to the parent base metal [99, 100]. High-purity ferritic filler metals are recommended when welding high-purity alloys, so that adequate toughness is maintained; however, good ductility and toughness can also be produced with Ni-based filler metals [98, 101].

2.2.2 Fluid flow in stainless steel welds

Four main forces contribute to the fluid flow in stainless steel welds: *Marangoni* forces, electromagnetic (*Lorentz*) forces, buoyancy forces and aerodynamic drag forces [102].

Marangoni forces arise mainly from the temperature-dependent surface tension gradients that exist in the weld pool. Fluid flow tends to be directed up the surface tension gradient. For example, in pure Fe and low-impurity steels, the surface tension increases as the temperature decreases, i.e., the temperature coefficient is negative. This leads to radially outward fluid flow and poor weld penetration. However, when the surface-active group 16 elements (S, O, Se, etc.) are present in the melt, the temperature coefficient of the surface tension can change to positive, leading to radially inward fluid flow in the molten weld pool [102–104]. For example, only 60 ppm of S is needed to change the temperature coefficient to positive and change the flow towards the centre and bottom of the weld pool [102]. This thermocapillary-driven fluid flow theory, initially proposed by Heiple and Roper [103, 105] for stainless steel welds, is generally accepted to be the main factor affecting fluid flow of the weld pool. Inward fluid flow is very beneficial in welding, as it leads to high weld penetration and productivity.

One would assume that alloying enough S to satisfy good productivity would be the norm. However, sulphides are generally regarded as detrimental to corrosion resistance, and they also impair hot workability and cold forming properties [106, 107]. Also, very stable sulphide and oxide forming elements, such as Ca, Al, and Ti, originating from the steelmaking can also reduce the available S and O by forming very stable CaO, CaS, Al_2O_3, TiO_2, etc. These compounds can survive in molten weld pool temperatures (1600–2100 °C), reduce the available surface-active elements, and alter the surface tension properties. Thus, very low S content and formation of very stable oxide inclusions can practically eliminate free S and O and impair weld penetration. In practical welding, there are techniques to overcome poor weld penetration such as using keyhole welding processes, hydrogen shielding or double shielding welding methods, or active flux gas tungsten arc (A-TIG) welding [104].

Even though Marangoni forces are usually considered to be the dominant forces for controlling weld penetration, other forces can have significant effects. Higher welding currents increase the electromagnetic forces and current density in the anode area [108]. Welding using high currents may also impose stirring effects in the weld pool [109]. Due to buoyancy effects, the hotter parts of the weld pool

gravitate towards the top of the weld and thereby influence fluid flow. Aerodynamic drag forces arise from arc pressure, high welding currents depress the surface of the molten metal and may improve penetration.

The overall combined effects of the above forces are complicated due to the interactions of the various welding parameters. For example, in the relatively simple autogenous GTA welding process, the following can also affect the fluid flow: the distance and inclination of the welding electrode to the workpiece, the tip geometry of the electrode, welding speed, the shielding gas used, and slag islands that may exist in the weld pools [108].

2.2.3 Slag island formation in welding

In the presence of free O, the elements originating from, e.g., scrap, refractories, deoxidation, desulphurization, inclusion shape control and stabilization practices such as Al, Ca, Mg, Mn, Si and Ti tend to form oxides. If these oxides survive in the molten weld pool, the particles can float to the surface of the weld pool due to buoyancy and accumulate as *slag islands* [106]. These slag islands (also known as slagging, slag spots, white spots, black spots, silicate islands, oxide islands, scum, rafts, films, patches, and refractory oxides) are often visible after welding and can also be found on the underside of the weld [106, 110].

Slag islands are not just an aesthetic inconvenience; the formation of large oxide clusters can alter the surface tension properties of the weld pool and interfere with the welding arc [106, 110–113]. Slagging is reported to cause arc instability, uneven weld bead, discontinuities, reduced and irregular penetration [106, 110–112, 114]. Slag islands may also promote corrosion problems, although this is controversial [113, 114]. It is also speculated that ferritic solidification mode might reduce slagging tendency due to the higher solubility of Ca, Si, Al, Ti and Zr in ferrite than in austenite [112].

Visible slag islands in certain grades and applications are frequently the subject of customer complaints. Depending on the customer processes, the requirements may vary considerably. For example, in semiconductor applications, visual slag formation is not allowed, as it may lead to contaminations [113]. In long tubular manufacturing, the weld should be free from imperfections for many hundred meters. Removal of slag islands can be costly and sometimes impossible due to unreachable joint configurations. Also, some manufacturers use rollers after welding, and rolled-in slag islands can leave a pit after pickling [106].

2.2.4 Solidification of ferritic stainless steel welds

Unlike austenitic stainless steels that have many solidification modes, ferritic stainless steels solidify to single-phase ferrite. The solidification structure starts to form as epitaxial nucleation from the partially melted HAZ grains at the fusion boundary. The solidifying grains align themselves in the <100> crystal growth direction. Grains that are aligned best to the solid-liquid interface of the weld pool will consume other grains via competitive growth [115]. Epitaxial growth from the fusion boundary can become disturbed if the chemical composition of the filler metal used is significantly different from that of the base metal. Compositional diversity can impose a barrier for nucleation, e.g., when ferritic stainless steels are welded with austenitic filler metals, and this leads to a characteristic interphase boundary [115].

Welding speed changes the shape of the weld pool and influences solidification. As the solidification follows the solid-liquid interface, the teardrop-shaped weld pool associated with higher welding speed can lead to pronounced impingement of columnar grains at the weld centreline. Impurities accumulate along the centreline, which can cause hot cracking. A more favourable solidification structure occurs with an elliptical weld pool, where the orientation of grains constantly changes, so that they maintain the alignment with the solid-liquid interface. However, very long unwanted axial grains may be more prominent with elliptical-shaped weld pools [116]. In ferritic stainless steels, the dendritic solidification substructure is generally not seen due to rapid back-diffusion after solidification [117, 118].

Solidification morphologies further change due to changes in constitutional supercooling. This is influenced by the temperature gradients and changes in the local liquidus temperatures. High-temperature gradients promote planar and cellular morphologies, whereas low-temperature gradients promote dendritic solidification. Alternative solidification processes occurring ahead of the solidifying front in the weld pool are dendrite fragmentation, grain detachment, heterogenous nucleation on secondary particles and surface nucleation [116]. The nucleation of grains on secondary particles, i.e., inoculation, is very effective and often used in metal casting [119]. In the case of steels, the effective nucleating agents vary with steel composition due to differences in the balance of interfacial energies between the nucleant, nucleus and the liquid metal [120]. The lowest calculated misfit between ferrite and secondary particles is with Ce oxides and sulphides, but generally, Al, Mg, Ti and Zr compounds are used in the refinement [118, 120, 121].

2.2.5 Microstructure after welding

Because of the broad chemistry range of ferritic grades, as evidenced by, for example, the ferrite factor given in Table 1, there are grade-dependent features in the welds that must be taken into consideration. The dual-phase structure of ferrite plus grain boundary martensite typically seen with high-interstitial unstabilized grades is usually detrimental regarding toughness, ductility and corrosion resistance [83]. A PWHT is preferred to temper the martensite [13]. However, the treatment should also be carried out at a high enough temperature (>750 °C) to allow Cr diffusion into the sensitized regions to restore the corrosion resistance. Lower interstitial contents may prevent the partial phase transformation to austenite, or the martensite that forms may be more ductile [122–125]. Regardless of the improved ductility, fully ferritic unstabilized grades can still suffer from sensitization after welding or other heat treatments.

The stabilized ferritic grades behave relatively similarly to each other in welding due to the absence of austenite formation. The entrapment of interstitials to e.g. Ti and Nb carbonitrides suppresses the formation of austenite at high temperatures. Subsequently, these alloys can be fully ferritic at all points of the welding thermal cycle. Practically, the only distinctive feature in welds of stabilized grades is the grain growth in the HAZ. The stable precipitates can restrict grain growth by pinning the grain boundaries [126, 127]. The effect is dependent on many factors, including particle type, shape, size, spacing and volume fraction [128]. The toughness of the stabilized welds is usually improved from that of unstabilized high interstitial welds but the ductile-brittle transition temperature (DBTT) could easily be near or at room temperature at moderate thicknesses (3.2 mm or 1/8 inch) in intermediate purity grades [129]. However, in high-purity alloys that have very low interstitial levels, even 12 mm thick plates have been shown to be feasible for welded structures [130].

3 Experimental

3.1 Materials

In total, 55 different ferritic stainless steel heats were examined; see Table 2 for the broad overview and individual papers for detailed chemical compositions. 49 heats were 11–21 wt.% Cr commercial heats from three stainless steel producers and at least four different melt shops. The remaining six heats were stabilized 21 wt.% Cr steels made in the laboratory. All the stabilized steels (n=49) can be considered as having intermediate purity, i.e., the sum of C and N was on average 0.04±0.01 wt.%. The unstabilized steels 1.4003 and 1.4016 (n=6) were used as a reference. Material thicknesses were in the range of 1.5–6 mm, four steels were in the hot rolled and annealed condition, and the rest of the materials were in the cold rolled and annealed condition.

Table 2. Broad overview of the test materials used (wt.%).

Steel grade	n	C	Si	Mn	Cr	Ni	Mo	Ti	Nb	Cu	N	Al
EN 1.4003	3	0.01-0.02	0.3	1.4	11.2-11.4	0.4	0.01-0.04	–	–	–	0.01	–
EN 1.4512	1	0.01	0.7	0.4	11.4	0.1	0.01	0.20	–	–	0.01	–
EN 1.4016	3	0.02-0.06	0.3-0.4	0.3-0.5	16.1-16.3	0.1-0.2	0.01-0.2	–	–	–	0.03	0-0.01
EN 1.4509	37	0.01-0.03	0.4-0.6	0.3-0.5	17.5-18.3	0.1-0.4	0.01-0.05	0.11-0.17	0.37-0.49	–	0.01-0.03	0-0.09
EN 1.4521	2	0.01-0.02	0.4-0.5	0.4-0.5	17.7-18.0	0.2-0.3	2.0-2.1	0.13-0.17	0.33-0.43	–	0.01-0.02	0-0.01
EN 1.4621	1	0.01	0.2	0.2	20.6	0.2	0.02	0.01	0.45	0.4	0.01	0.00
EN 1.4622	2	0.02	0.5-0.6	0.4	20.8	0.2	0-0.02	0.12-0.15	0.25	0.3-0.4	0.02	0.01-0.01
21Cr Lab	6	0.02-0.03	0.4-0.5	0.3-0.5	20.2-21.1	0.2-0.8	–	0.02-0.53	0.01-0.54	0.4	0.01-0.02	0.01-0.05

Papers I and II investigated 31 materials in the 1.5 mm nominal thickness from the stabilized steel grade 1.4509. Paper III included one heat from 1.4003, 1.4512, 1.4016 and 1.4509 grades, all in 2 mm thickness. Paper IV contained all commercial materials, excluding those from Papers I and II. Paper V investigated four stabilized laboratory steels in 3 mm thickness, and Paper VI the remaining two 2 mm laboratory steels and one 1.5 mm commercial steel of grade 1.4622.

The laboratory steels were melted with varying amounts of Ti, Nb and Al. Materials were reheated at 1100–1115 °C, then hot rolled using approximately 30% reduction per pass to 5 mm and subsequently cold-rolled to 2–3 mm, then annealed in the range 925–1030 °C and pickled. In addition, the welds in Paper VI were produced with wet ground 600 grit finishes to ensure comparable surface conditions.

3.2 Methods

Several welding processes and techniques were used in this research work and these are summarized in Table 3. A brief explanation is provided here and a more detailed description can be found in the corresponding papers.

Table 3. Preparation techniques used.

Preparation technique	Paper I	Paper II	Paper III	Paper IV	Paper V	Paper VI
GTA welding	X	X		X		X
GMA welding			X	X		
SMA welding				X		
Laser welding				X		X
Gleeble simulation				X	X	
PWHT			X			
Shielding gas mixing		X				X
Parameter monitoring		X				

Mechanized autogenous bead-on-plate GTA welding was used with a variety of welding parameters. In Paper I, five different GTA welding scenarios were used to produce a variety of 200 mm in length partial penetration and full penetration welds for slag island and weld penetration evaluations. Paper II continued the research with *in situ* weld pool characterization, continuous welding parameter monitoring and additional welding scenarios that also introduced 3% H_2 to the typical Ar shielding. In Paper III, mechanized square butt welding experiments were carried out using pulsed GMA welding and Ar + 2% O_2 shielding for 2 mm materials with Ø 1 mm solid core ferritic (409LNb, 430LNb and 430Ti) and austenitic (308LSi) filler wires. In addition, PWHTs were investigated according to the standard or filler wire manufacturer recommendations at 750 °C for 1 to 2 hours. Paper IV combined the data from 1.5–6 mm materials of multiple welding techniques, including GTA, GMA, SMA welding, laser welding and Gleeble HAZ thermal simulations. Paper V used further Gleeble simulations to produce variations in the

HAZ microstructure with different heat inputs (0.3, 0.5 and 0.9 kJ/mm) at peak temperature of 1350 °C for 3 mm materials. Finally, Paper VI used GTA and laser welding and mixtures of shielding gases (Ar, O_2 and N_2) to investigate the possibilities of encouraging grain refinement in the weld metals of 1.5–2 mm thick materials.

Various mechanical and corrosion tests were used to assess the feasibility of welds prepared in Papers III–VI. Table 4 lists the testing methods and the corresponding papers provide more details.

Table 4. Testing methods used.

Testing method	Paper I	Paper II	Paper III	Paper IV	Paper V	Paper VI
Hardness			X		X	
Impact toughness			X	X	X	X
Tensile testing			X	X		X
Erichsen testing			X			
Cracking resistance						X
Oxidation testing						X
Intergranular corrosion						X

Papers I and II did not contain material property testing. Paper III compared welds produced with ferritic and austenitic filler metals using various mechanical tests: room temperature tensile tests, hardness evaluations (HV1 and HV0.1), impact toughness testing (-40 °C to +20 °C) and Erichsen cupping tests that were used to evaluate the stretch formability of the welds. Paper IV correlated extensive impact toughness test data to fracture appearance in 17 materials and their welds. Yield strengths of the base materials are provided for reference. In Paper V, various Gleeble simulated HAZs were investigated via impact toughness (-60 °C to +80 °C) and hardness (HV1) testing. High-temperature tensile and oxidation tests (900 °C), impact toughness tests (-20 °C to +40°C), Houldcroft-type fishbone solidification cracking tests and Strauss intergranular corrosion testing were used in Paper VI to assess the properties of experimental fine-grained welds compared to those of the ordinary columnar-grained welds.

Multiple characterization techniques were used throughout this research work. Table 5 gives an overview, and detailed descriptions are provided in the corresponding papers.

Table 5. Characterization techniques used.

Technique	Paper I	Paper II	Paper III	Paper IV	Paper V	Paper VI
LOM / LCF	X		X	X	X	X
SEM	X	X	X	X	X	X
SEM-EDS	X	X	X	X	X	X
SEM-EBSD						X
STEM					X	
STEM-EDS					X	
Visual	X	X				
In situ OE		X				
Video imaging		X				

Light optical microscopy (LOM), laser confocal microscopy (LCF) and scanning electron microscopy (SEM) with accompanying modules were the primary characterization techniques. In Paper I, visual inspection was used to determine the extent of slagging intensity and LOM/LCF was used to assess the level of weld penetration. SEM with energy-dispersive X-ray spectrometry (EDS) was used for analysing the chemical compositions of slag islands. Paper II continued the work and included weld pool video imaging and *in situ* optical emission spectroscopy. In Paper III, LOM/LCF was used to distinguish the amount of dilution and microstructural differences between welds produced with different filler metals. In addition, SEM-EDS was used to analyse the secondary phases observed after PWHT. In Papers IV–VI, LOM/LCF was used for main microstructural characterization, SEM-EDS was used for fractography and particle analysis for particles $\geq Ø$ 1 µm. In Paper V, the scanning transmission electron microscope (STEM) combined with EDS was used for particle analysis below $Ø < 1$ µm after electrolytic extraction. Electron backscattering diffraction (EBSD) was used in Paper VI for phase recognition.

Statistical analyses were carried out mainly using multiple linear regression. Analysis and models were prepared in Papers I, II and V. To minimize the sensitivity to data outliers, typically, a limit of plus or minus two standard deviations were used for the residuals. Variance inflation factor (VIF) was used to assess the multicollinearity of the independent variables. Collinear variables (VIF > 5) were treated so that the variable with the strongest relationship was included in the final model.

4 Results

4.1 Slagging assessed after welding

The formation, development and influence of slag islands were studied in Papers I and II for 31 commercial steels of grade 1.4509. In Paper I, the slagging was studied in four autogenous GTA welding scenarios after welding by using a visual ranking system and SEM-EDS. For the 200 mm long welds, the visual slagging intensity criteria were: 0 = no slag observed, 1 = two-millimetre-scale large spots and a few small spots allowed, 2 = less than 5 large spots or < 20% continuous slag along the weld, 3 = less than 10 large spots or 20–50% continuous slag along the weld, 4 = countless large spots or 50–100% continuous slag along the weld, 5 = weld entirely covered by slag or countless large spots with 100% continuous slag.

Based on the visual inspection, two different slag types were identified: bluish glassy slag associated with arc ignition and globular slag spots. Multiple linear regression models were derived to estimate the slagging intensity (Table 6). The analysis indicated that of the 15 elements analysed (C, Si, Mn, P, Cr, Ni, Mo, Ti, Nb, Cu, N, S, Al, Ca, O), Al promoted ignition slags, whereas Ca and Ti generally promoted slag spots.

Table 6. Regression analysis of the slagging intensity (0–5). [Paper I, modified and reprinted by permission of Springer]

Test series	Slag types analysed	Variable	Coeff.[3]	VIF[4]	n	R^2 adj.	SE[5]
D/W[1]	No slag and ignition slags	(Const.)	-0.43	-	24	98%	0.21
		Ca[8]	-418.9	1.03			
		Al[8]	85.55	1.03			
D/W[1]	Ignition slags	(Const.)	-15.61	-	16	80%	0.56
		Al[7]	39.70	1.11			
		Voltage[8]	1.61	1.11			
D/W[1]	No slag and slag spots	(Const.)	-4.60	-	55	70%	0.89
		Ca[8]	2127	1.06			
		Ti[8]	31.98	1.06			
D/W[1]	Slag spots	(Const.)	-4.03	-	37	70%	0.75
		Ca[8]	1859	1.14			
		Ti[8]	44.3	1.38			
		Al[8]	-100.2	1.33			
W_b/W_f[2]	Slag spots	(Const.)	2.91	-	22	48%	0.85
		Ca[6]	745	1.05			
		Al[8]	-73.8	1.05			

[1] D/W = partial penetration welding scenarios, [2] W_b/W_f = full penetration welding scenarios, [3] regression coefficients, [4] variance inflation factors, [5] standard error of the regression models, [6] $p < 0.05$, [7] $p < 0.01$, [8] $p < 0.001$

SEM-EDS analyses were carried out on 226 individual slag islands. For quantitative chemical analysis, EDS spectra were corrected by assuming that there was no Fe in the slag and that the Fe signal originated entirely from the steel matrix. The upper limit for the matrix contribution was set to 70%. In this way, it was possible to correct the measured compositions by subtracting the matrix composition weighted according to the apparent Fe content measured. In addition, a 5 wt.% threshold value was set to the elements present in the slag to minimize any artefacts coming from the normalization. The main elements found in slag islands were O, Ca, Ti and Al, as listed in Table 7. Chromium was also quite frequently present, but it was thought to be an artefact of the EDS correction process, originating mainly from the matrix rather than the slag islands.

Table 7. Summary of the main elements found in 226 slag islands. [Paper I, modified and reprinted by permission of Springer]

Element	O	Ca	Ti	Al	Cr	Zr, Mg, N, Nb, C, Si, Mn, S, P
Count ≥5%[1]	226	210	203	155	52	≤ 10
Frequency, %[2]	100	93	90	69	23	< 5
Min, wt.%	12	5	5	5	5	–
Mean, wt.%	35	22	22	23	10	–
Max, wt.%	49	47	61	48	17	–

[1] number of particles greater or equal to the 5 wt.% threshold value, [2] frequency of an element with respect to the total number of slag islands analysed

An example of a large mm-scale slag spot is shown in Fig. 1 together with EDS elemental maps of Al, Ca and Ti. Fig. 2 shows how a slag spot is seen on top of an Al raft and how it has influenced the fusion boundary. Fig. 3 shows an example of non-crystalline glassy slag island. In the figures, the compositions calculated from the EDS spectra are not normalized. There was a general trend that an increase in the bulk Al increased the amount of Al seen in the slag islands, as shown in Fig. 4.

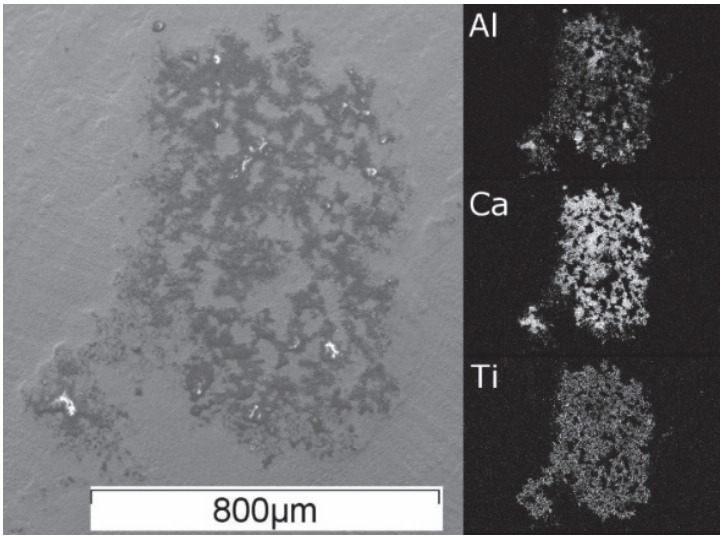

Fig. 1. Example of EDS-mapping of a large slag island. [Paper I, reprinted by permission of Springer]

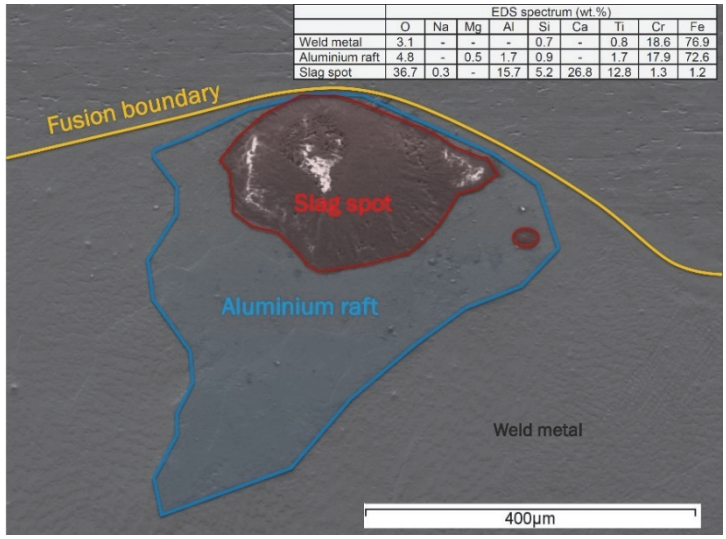

Fig. 2. Example of slag island characteristics and raw EDS spectra. [Paper I, reprinted by permission of Springer]

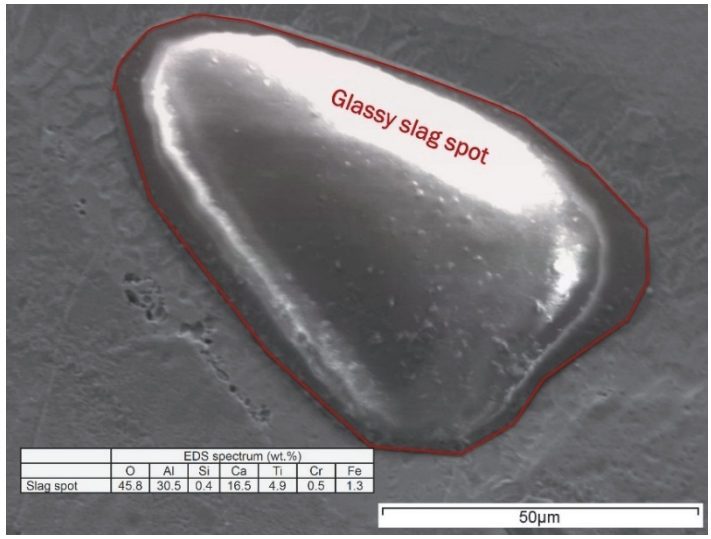

Fig. 3. Example of a glassy slag island and raw EDS spectrum. [Paper I, reprinted by permission of Springer]

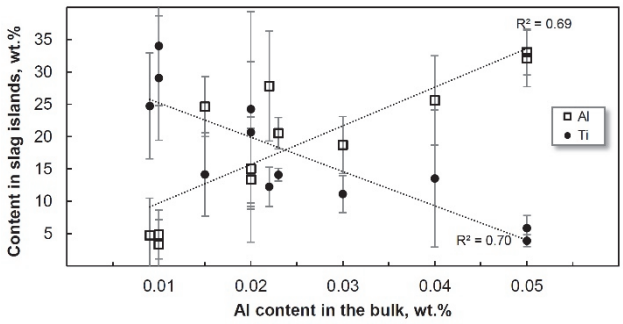

Fig. 4. Changes in the composition of slag islands with respect to Al in the bulk. [Paper II, modified and reprinted by permission of Springer]

4.2 Slagging assessed *in situ*

In Paper II, the slagging characteristics were examined in more detail. Various additional autogenous GTA welding scenarios were prepared and examined by using weld pool video imaging, *in situ* optical emission spectroscopy, welding parameter monitoring and metallography. Based on observations from about 120 welds, three separate slagging mechanisms were identified and these could be correlated to the chemical composition of the steel and welding parameters used (Fig. 5a–c). In addition, based on the movement of slag particles, typical fluid flow patterns were approximated (d).

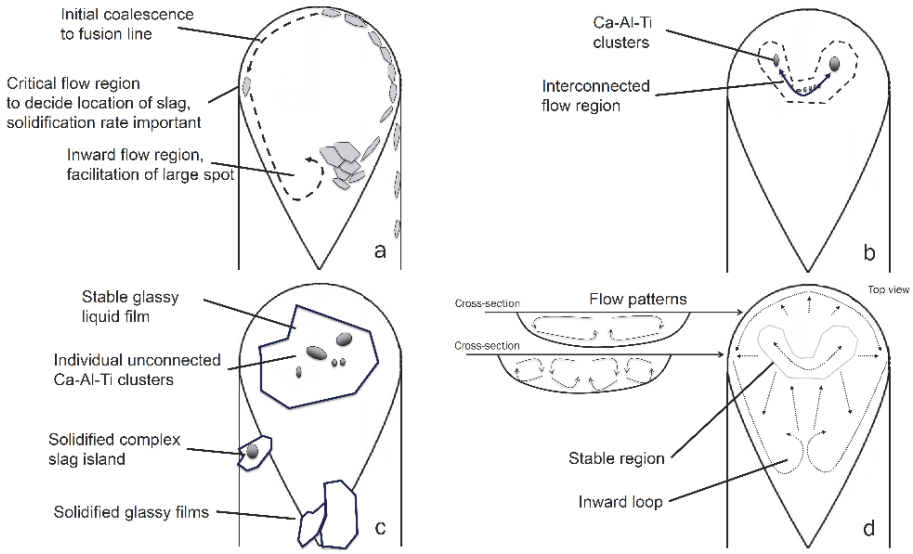

Fig. 5. Proposed mechanisms for slagging phenomena; accumulation of slag spots at the sides and rear of the weld pool (a), Ca-Al-Ti cluster formation (b) and large Al-based film formation (c). Fluid flow patterns are implied from the observed movements of slag islands (d). The shape of the weld pool may vary from elliptical to tear drop depending on the welding parameters used. [Paper II, reprinted by permission of Springer]

The most visually striking slag islands, globular slag spots, (Fig. 5a) were the result of slag accumulated at the rear of the weld pool. This slag type was more prominent in low-Al, high-Ca steels. The build-up occurred as the initial outward fluid flow, a characteristic of low S steels, kept the small slag particles close to the fusion line. Depending on the weld solidification front, the small slag particles would either adhere to the edges of the weld or accumulate at the rear of the weld pool, where a distinct inward flow was detected in most welding scenarios from the video footage. Once the slag spot grew to a size where it would touch the solidifying front, it detached from the weld pool and often formed mm-scale slag spots like those presented in Fig. 1. However, not all slag would detach at once, as some residue of the spot would facilitate the development of a new spot. This residue also prevented the formation of smaller slag spots at the rear, sometimes seen at the beginning of the weld, where two separate slag accumulations would take place in the inward loop of the flow at the rear of the weld pool, Fig. 6. The inward flow region would further promote the development of new large spots instead of small spots, Fig. 7.

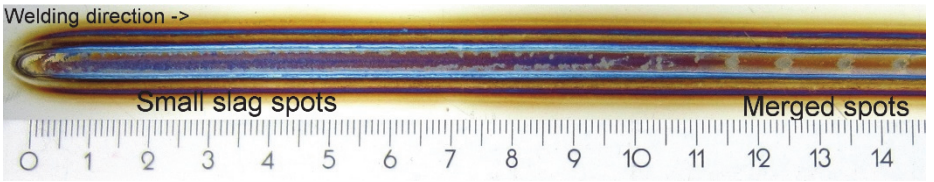

Fig. 6. Merge of slag islands (scale in cm). [Paper I, modified and reprinted by permission of Springer]

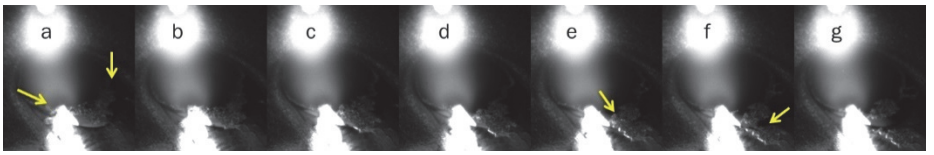

Fig. 7. Build-up of slag at the rear of the weld pool, and slag detachment. [Paper II, reprinted by permission of Springer]

The second slag type (Fig. 5b) consisted of small < Ø 1 mm black spots that had a mean chemical composition of 22 ± 12% Al, 21 ± 8% Ca and 14 ± 9% Ti. These spots would develop more frequently in high-Ca steels. Typically, these black spots would travel at about one fourth of the distance from the fusion line towards the centre of the weld pool. The black spots would frequently exist at these one-fourth locations, and fluid flow patterns implied that these were relatively stable locations. However, once the flow patterns were disturbed, the black spots would very quickly, in roughly 50 ms, i.e., at 0.04 m/s, be drawn to the fusion line, where local fusion line discontinuities would form, as seen in Fig. 8 and previously presented Fig. 2.

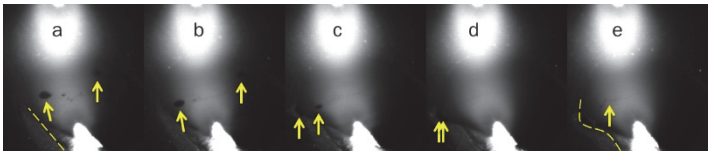

Fig. 8. Black spot movement and fusion line discontinuity. [Paper II, reprinted by permission of Springer]

The third slag type (Fig. 5c) was thin but comparatively large glassy film oxide mostly comprised of Al (~49 wt.%) that also contained some Ti (~15 wt.%), the remainder being O. These films were found more frequently as the Al concentration

increased and were analogous to the post-welding ignition slags presented in Paper I. Owing to the thin and transparent nature of the film, clear visual distinction *in situ* was limited to a few welds. However, it was clear that these films could cover the entire front part of the weld pool and survive through the weld cycle, as seen in Fig. 9. Films also disturbed the movement and adherence of black spots.

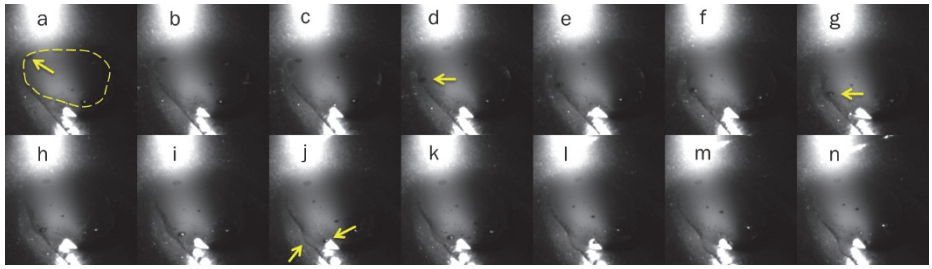

Fig. 9. Film formation. [Paper II, reprinted by permission of Springer]

Based on *in situ* examinations, it became very clear that slag island examinations after welding can be misleading. The visual ranking of slag islands was mainly limited to large slag spots that accumulated and eventually detached at the rear of the weld pool. These post-welding investigations were not able to distinguish the influence and existence of black spot clusters and glassy films during the welding.

Welding parameter monitoring showed that most notable changes during welding occurred with arc voltage. Occasionally, it appeared that heavy slag island formation influenced the measured arc voltage. However, this type of behaviour was not consistent and had no statistical significance in regression analyses. Regression models about the factors influencing arc voltage were also inconsistent between different welding scenarios. Optical emission spectroscopic examinations from the welding arc revealed that Ar I intensity generally has a good correlation to momentary arc voltage. The optical emission spectra also contained Ca, Mn and Na peaks. However, no clear interactions between slagging and spectroscopy could be identified with the set-up and analysis techniques used.

Slagging intensity was successfully lessened by using a reducing shielding gas (Ar + 3% H_2), but this generally only offered minor improvements. Pulsed current technique induced a rocking motion to the weld pool and disturbed the typical solidification behaviour. However, the effect of pulsed current on the slagging intensity was dependent on welding parameters, i.e., the slagging would diminish

or increase depending on how the parameters influenced the solidifying front, the weld pool geometry and subsequent slag accumulation mechanisms.

4.3 Weld penetration studies

In Paper I, the level of weld penetration was studied in 31 commercial steels of grade 1.4509 in five autogenous GTA welding scenarios. The scenarios consisted of partial penetration (D/W) and full penetration welds (W_b/W_f). In about 22% of the welding test cases, changing weld penetration profile was observed along the length of the weld. The criterion for changing penetration was set to the relative standard deviation of 10%. Values above this limit were not included for penetration studies. Among those accepted, a clear trend existed that trace amounts of Ca degraded the penetration in every scenario, as seen in Fig. 10. However, statistical analyses showed that when considering the minimum-maximum ranges of the elements, Ti and Si were equally important in controlling the penetration (Table 8). The level of penetration was generally modest, for example, in partial penetration welds, 72% were below 0.30, which is generally regarded to be the limit for poor weld penetration. The surface-active elements S and O had no statistical effect on penetration for the ranges studied.

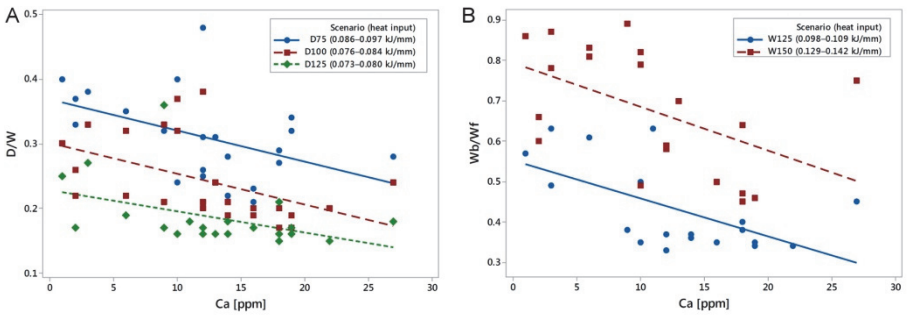

Fig. 10. Simple relationships between Ca content and weld penetration measured using partial penetration depth-to-width ratios (D/W) (A) and for full penetration welds, the ratio of the weld root bead width to weld face width (W_b/W_f) (B) [Paper I, reprinted by permission of Springer]

Table 8. Regression analyses of the penetration tests. [Paper I, modified and reprinted by permission of Springer]

Test series	Variable	Coeff.	VIF	Range[3]	Max effect[4]	n	R^2 adj.	SE
D/W[1]	(Const.)	-0.88	–	–	–	52	91	0.02
	Ca	-14.45	1.22	0.0025	16%			
	Ti	-0.77	1.26	0.06	21%			
	Si	-0.12	1.20	0.26	14%			
	Cr	0.03	1.07	0.7	10%			
	Heat input	8.61	1.15	–				
W_b/W_f[2]	(Const.)	0.95	–	–	–	27	97	0.03
	Ca	-128.6	1.52	0.0026	63%			
	Ti	-4.79	1.28	0.04	36%			
	Si	-1.46	1.34	0.21	58%			
	Al	3.19	1.56	0.037	22%			
	Heat input	9.09	1.05	–	–			

Shielding gas Ar 15 l/min, Backing gas Ar 10 l/min, gas cup Ø no 7, DCEN, GTA efficiency 0.6, electrode stick-out 6 mm, distance to workpiece 2 mm, Ø2.4 mm WTh-2 electrode, 45° tip angle, truncation diameter 0.19±0.04 mm; [1] D/W = three partial penetration welding scenarios: 75 A 9.5–10.8 V 300 mm/min, 100 A 10.2–11.3 V, 483 mm/min and 125 A 11.0–12.0 V 675 mm/min; [2] W_b/W_f = two full penetration welding scenarios: 125 A 10.5–11.7 V 483 mm/min, and 150 A 11.5–12.7 V 483 mm/min; [3] wt.%; [4] estimated maximum effect as a percentage of the mean value: D/W=0.22, W_b/W_f=0.53

4.4 Microstructure and properties

Weld metal microstructures were examined in Papers III, IV and VI. Heat-affected zones were examined mainly in Paper V but also to some extent in Papers III and IV.

4.4.1 Influence of filler metals

In Paper III, two stabilized (1.4512, 1.4509) and two unstabilized 2 mm thick ferritic grades (1.4003, 1.4016) were GMA welded using Ø 1 mm solid-core stabilized ferritic filler wires (409LNb, 430LNb, 430Ti). Austenitic filler metal (308LSi) was used as a reference. Basic mechanical properties were evaluated: hardness, tensile, impact toughness and weld area ductility via the Erichsen cupping test. The welds were characterized using LOM and SEM-EDS, and the weld metal microstructures were estimated using stabilization and ferrite factor calculations. The amount of dilution was estimated from the micrographs. Possible

pick-up reactions or element loss during welding were not considered in the calculations.

The microstructures could be roughly estimated with the use of a modified ferrite factor that included Nb as a ferrite former. The welds in unstabilized 1.4003 using 409LNb filler wire had a ferrite factor of about 11 and contained a significant amount of martensite. In the low Cr stabilized steel 1.4512, some minor amounts of martensite were present due to the ferrite factor being just above 13.5, which is the limit for fully ferritic welds. The medium Cr steels 1.4016 and 1.4509 generally did not show martensite in the welds, but steel 1.4016 welded using high interstitial 430Ti filler wire contained minor amounts of grain boundary martensite. Martensite was generally harmful for the toughness and ductility of the weld and HAZ, excluding the superior toughness properties achieved in welds of unstabilized steel 1.4003.

Regardless of the presence of martensite, the most distinct feature in the micrographs was the coarse columnar grains that were particularly obvious in welds fabricated with the Nb-stabilized filler metals 409LNb and 430LNb, seen in Fig. 11. Even in the absence of martensite, very low impact toughness values were seen in most of these coarse-grained welds, with DBTT values being 0 °C for 409LNb welds and above 40 °C for 430LNb, excluding the values in welds of steel 1.4003. Some grain refinement and improvements in toughness were seen with welds fabricated with Ti-stabilized wire.

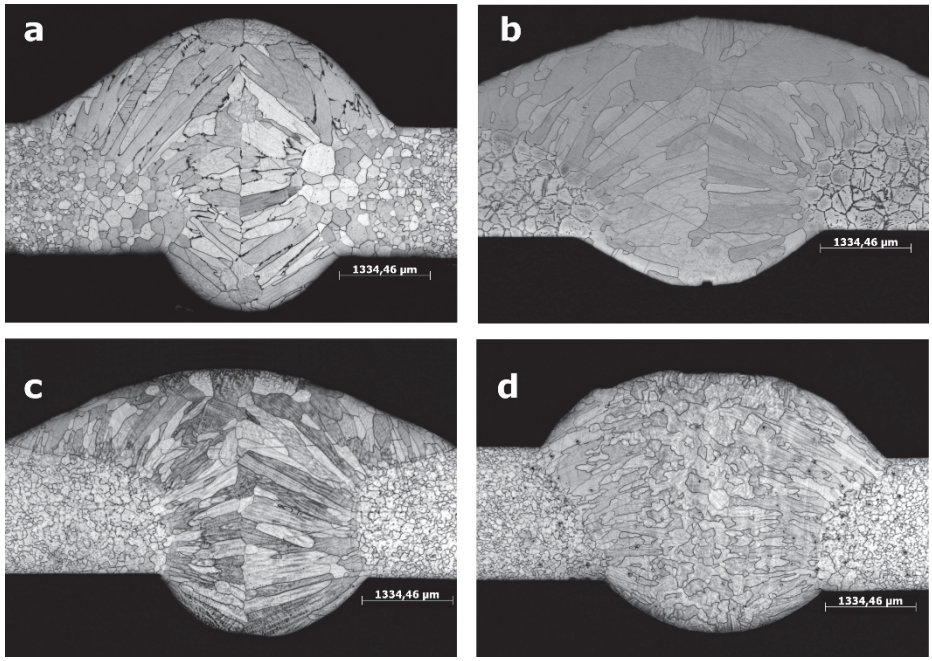

Fig. 11. Microstructures of welds using ferritic filler metals; 1.4512 & 409LNb (a), 1.4016 & 430LNb (b), 1.4509 & 430LNb (c), 1.4509 & 430Ti (d). [Paper III, modified and reprinted by permission of Springer]

Regarding other properties, the tensile strength of the welds generally surpassed that of the base metals. A PWHT tempering carried out at 750 °C for 1 to 2 hours generally improved ductility in Erichsen testing but relocated the rupture in tensile testing into the weld metal. It was also demonstrated that unnecessary PWHT for steel 1.4509 runs the risk of inducing the Laves phase in the base metal and HAZ with a noticeable reduction in impact toughness, as seen in Fig. 12.

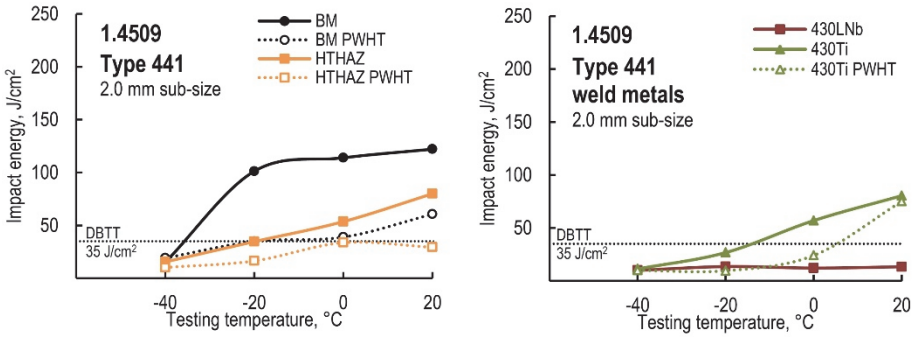

Fig. 12. Impact toughness of 1.4509 welds using 430LNb and 430Ti filler wires. BM denotes base metal, HTHAZ denotes high-temperature HAZ, DBTT denotes the ductile-brittle transition temperature for sub-sized specimens. [Paper III, modified and reprinted by permission of Springer]

4.4.2 Grain refinement in autogenous welds

In Paper VI, efforts were made to induce grain refinement in 21 wt.% Cr-stabilized ferritic stainless steel autogenous GTA welds that would otherwise solidify in a columnar fashion. An approach was used in which Al and Ti needed to form oxides, and nitrides were introduced by alloying the steel, and the needed O and N for effective inoculation were introduced via the shielding gas.

Fig. 13 demonstrates that an experimental laboratory steel solidified in a columnar manner when using normal Ar shielding in GTA welding. A gradual grain refinement was achieved in the two experimental laboratory steels when the shielding gas was mixed with 1–10 vol.% N_2 and 0.5–3 vol.% O_2 components.

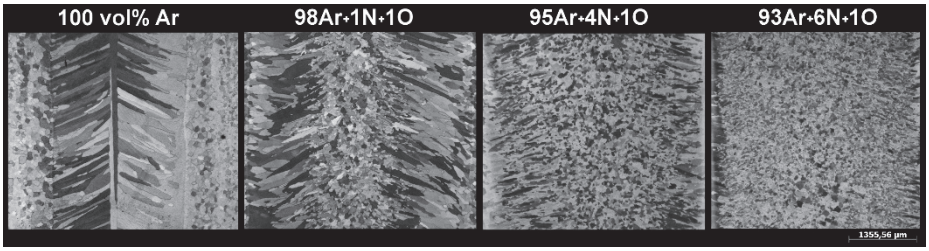

Fig. 13. Grain refinement using shielding gas mixtures in GTA welding, top view. [Paper VI, modified and reprinted by permission of Springer]

Grain sizes of about 40 µm were achieved at the weld centreline through the process, and the fraction of equiaxed grains increased with the increase of N_2 and O_2 components in the shielding gas (Fig. 14). The effect did not take place if the shielding gas was mixed with either N_2 or O_2 alone, although some irregularities in solidification were observed with single N_2 additions.

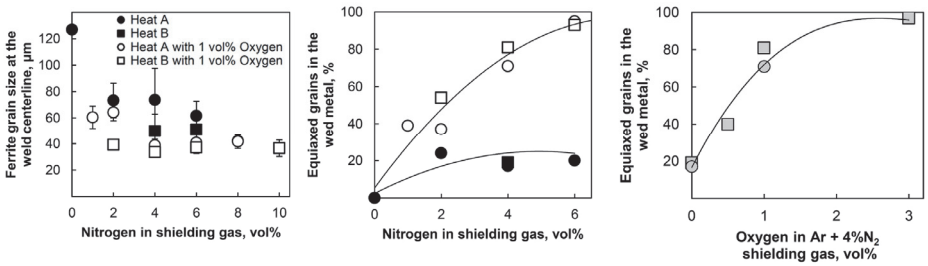

Fig. 14. Grain size and fraction of equiaxed grains in the welds with respect to N_2 and O_2 in shielding gas. [Paper VI, modified and reprinted by permission of Springer]

Grain refinement was unsuccessful in laser welding. Gas analyses from the weld metals indicated that nitrogen absorption had been very limited in laser welds compared to the GTA, seen in Fig. 15. The gas analyses also showed that oxygen was needed to produce surface slag that protected the weld metal from nitrogen outgassing. An interesting feature in some of the high N welds was the presence of retained austenite (15–20 vol.%) instead of martensite. The modified Schaeffler diagram of Espy [131] indicated that austenite could be stable in welds with more than about 0.1 wt.% N.

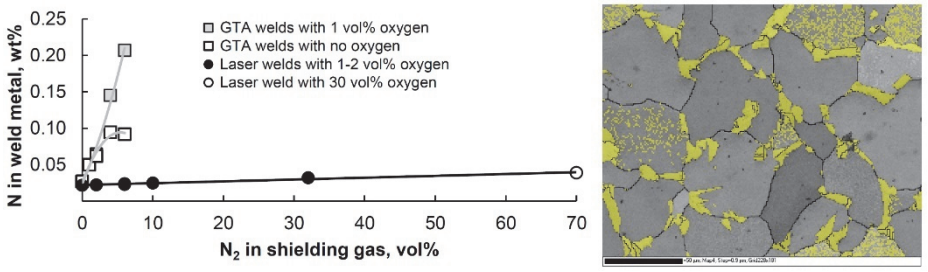

Fig. 15. The effect of shielding gases on the N content of the weld metals (left) and retained austenite observed in high N welds with SEM-EBSD (right). [Paper VI, modified and reprinted by permission of Springer]

The fine-grained welds showed mixed results in mechanical and corrosion testing. High-temperature tensile and oxidation resistance was at least comparable to those of columnar-grained welds. The cracking resistance of the welds assessed via fishbone-type specimens slightly improved with fine-grained welds. However, owing to the increase in interstitial content, impact toughness deteriorated with an increase in the DBTT by about 20 °C, and the welds were susceptible to intergranular corrosion. Retained austenite was seen to be slightly beneficial by preventing sensitization of ferrite-ferrite grain boundaries, but no improvements were seen in impact toughness.

4.4.3 Role of precipitates and inclusions with respect to toughness

In Paper V, the correlation between microstructure and toughness parameters was investigated in four 21 wt.% Cr-stabilized ferritic laboratory steel base metals and simulated HAZs. The steels had interstitial contents of 380–450 ppm by mass and the stabilization varied from fully Nb-stabilized to fully Ti-stabilized. Gleeble thermomechanical simulations were made with a peak temperature of 1350 °C by using three different heat input scenarios: low (0.3 kJ/mm), medium (0.5 kJ/mm) and high heat input (0.9 kJ/mm). The microstructures were evaluated via LOM/LCF, SEM-EDS and STEM. A feature detection routine was utilized in precipitate and inclusion particle analysis. The results were normalized by assuming that any Fe signal originated entirely from the steel matrix. The upper limit for the matrix contribution was set to 70%, and the minimum particle size was set to Ø 1 µm equivalent circle diameter (ECD). The analysed particles were grouped into various compound systems (Al_2O_3, TiO_2, TiN, NbN, TiC, NbC and $Cr_{23}C_6$), based on their dominant elements. For steel C, electrolytic extraction combined with SEM-EDS and STEM was used to analyse particles with Ø < 1 µm.

In Fig. 16, it is shown that although the initial microstructures varied between the steels, after the HAZ simulations, the microstructures became very similar, especially in higher heat input scenarios. The majority of large particle clusters originating from the processing vanished and were replaced with fine intragranular dispersion *clouds* of precipitates and intergranular grain boundary precipitates. The only clear difference was the absence of cuboidal Ti nitrides in Nb-stabilized steel A. The Ti nitrides were generally unaffected by the heat input and precipitates surrounding the nitride (presumably carbides) were dispersed into the vicinity.

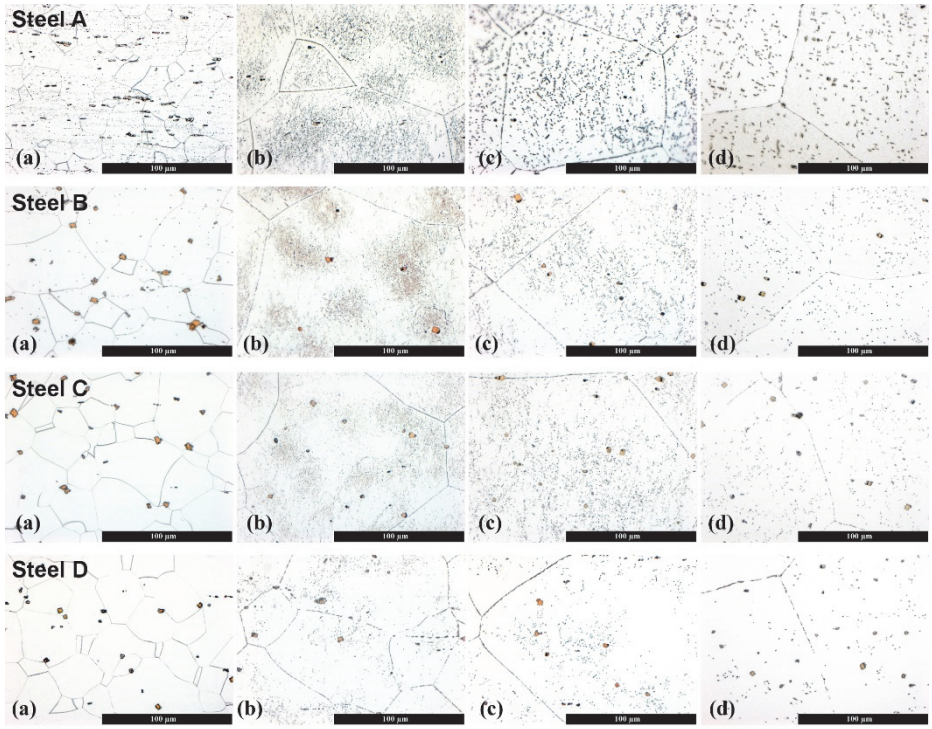

Fig. 16. Microstructures before and after thermal simulations in steels A–D; base metal (a), low heat input (b), medium heat input (c), high heat input (d). Steel A is Nb-stabilized, steels B and C are dual-stabilized, and steel D is Ti-stabilized. [Paper V, modified and reprinted by permission of Springer]

In the highest heat input scenario, the mean grain size increased to 6–10 times that of the base metal, i.e., from 19–31 µm to 180–210 µm, seen in Table 9. Hardness values were rather monotonous; the base metals had the lowest hardness. However, Nb-stabilized steel A showed a considerable increase in hardness with low heat input and a decline in hardness, as the cooling rate decreased with medium and high heat inputs. All in all, the DBTT range was 87 degrees, including the base metals and simulated HAZs. In the base metals, Nb-stabilized steel A showed the lowest and Ti-stabilized steel D the highest DBTT. An increase in the heat input generally increased the DBTT. Nb-stabilized steel A had the finest mean particle size, Ø 1.3–1.4 µm, whereas the other steels had similar mean particle sizes in the range Ø 1.9–2.2 µm.

Table 9. Basic characterization data for the examined steels. [Paper V, modified and reprinted by permission of Springer]

Steel	Heat input, kJ/mm	Grain size, µm	Hardness, HV1	DBTT[1], °C	USE[2], J/cm^2	Mean particle size, µm
A	Base	19 ± 3	154 ± 3	-35	155	1.3 ± 0.3
	0.30	74 ± 11	168 ± 3	4	150	1.3 ± 0.2
	0.50	106 ± 28	164 ± 2	-2	154	1.4 ± 0.3
	0.90	185 ± 21	159 ± 5	4	149	1.4 ± 0.4
B	Base	30 ± 7	152 ± 2	-17	177	2.1 ± 0.9
	0.30	94 ± 14	161 ± 3	-8	160	2.2 ± 1.0
	0.50	119 ± 28	155 ± 2	18	172	2.2 ± 0.9
	0.90	210 ± 39	155 ± 3	37	185	2.2 ± 0.9
C	Base	28 ± 4	153 ± 3	-5	167	1.9 ± 0.7
	0.30	95 ± 13	157 ± 5	14	157	2.0 ± 0.7
	0.50	124 ± 19	160 ± 3	28	166	2.0 ± 0.7
	0.90	180 ± 20	155 ± 5	52	171	2.2 ± 0.8
D	Base	31 ± 7	158 ± 4	12	147	2.1 ± 0.8
	0.30	96 ± 12	159 ± 3	22	145	2.0 ± 0.7
	0.50	127 ± 21	162 ± 3	11	151	2.0 ± 0.8
	0.90	182 ± 12	158 ± 4	45	154	2.2 ± 0.8

[1] ductile-brittle transition temperature, [2] upper shelf energy

Size distributions for the various particle types grouped according to the dominant compound in the particle are shown in Table 10. It must be emphasized that the groups are merely estimates concerning the dominant compound in the particles. Nevertheless, as observed in the micrographs, the absence of TiN-rich particles is apparent in steel A. Among noticeable differences between the materials were also the presence of TiC-rich particles in steel D and NbC-rich particles in steel A. Although all steels were deoxidized with Al, the EDS spectrum from the nitrides probably obscured the spectrum from an oxide core in steels B–D, unlike in steel A, where small Al_2O_3 particles were evident.

Table 10. Size distributions for the various particle types grouped according to the dominant compound in the particle. Number of particles per frame divided into size classes 1–1.9 µm / 2–2.9 µm / ≥ 3 µm. [Paper V, modified and reprinted by permission of Springer]

Steel	Heat input, kJ/mm	Al_2O_3	TiO_2	TiN	NbN	TiC	NbC	$Cr_{23}C_6$	Multiple
A	Base	5.1/0.2/-	4.2/0.1/-	-/-/-	0.8/-/-	-/-/-	41.7/2/0.2	0.9/0.1/-	2.5/0.1/-
	0.30	1.8/0.1/-	0.5/-/-	-/-/-	-/-/-	-/-/-	5.8/0.1/-	-/-/-	0.1/-/-
	0.50	2/0.1/-	0.2/-/-	-/-/-	0.1/-/-	-/-/-	5.2/0.3/-	-/-/-	0.3/-/-
	0.90	3.1/0.2/0.1	1.4/-/-	-/-/-	0.4/-/-	-/-/-	28.6/2/0.4	0.1/-/-	0.6/0.1/-
B	Base	0.1/0.1/-	0.1/0.1/-	3.6/1.5/1.2	-/-/-	-/-/-	-/-/-	-/-/-	0.3/0.1/-
	0.30	0.1/0.1/-	1.1/0.3/0.2	4.5/2.4/1.8	-/-/-	0.1/-/-	0.4/-/-	-/-/-	0.7/0.7/0.2
	0.50	-/0.1/0.2	0.6/0.2/0.1	3.8/2.5/1.8	-/-/-	-/-/-	-/-/-	-/-/-	1/0.7/0.2
	0.90	-/0.1/-	0.2/0.2/0.1	4.2/2.7/1.9	-/-/-	0.1/-/-	0.3/-/-	-/-/-	0.2/0.3/0.1
C	Base	0.1/0.1/-	-/0.1/-	6/3.1/0.7	-/-/-	-/-/-	-/-/-	-/-/-	0.1/0.1/0.1
	0.30	0.2/0.2/0.1	0.5/0.1/0.2	7.4/4.8/1.2	-/-/-	-/-/-	-/-/-	-/-/-	0.2/0.1/0.1
	0.50	1/0.6/0.2	0.8/0.4/0.1	7.8/4.2/1.1	-/-/-	0.1/-/-	-/-/-	-/-/-	0.9/0.4/-
	0.90	-/-/0.1	0.5/0.1/-	4.9/4.6/1.9	-/-/-	-/-/-	-/-/-	-/-/-	0.4/0.2/0.1
D	Base	-/-/-	0.1/-/-	0.2/1.4/0.9	-/-/-	8.8/5.2/0.7	-/-/-	-/-/-	0.2/0.5/0.6
	0.30	-/-/-	0.3/-/-	1.5/3.2/0.8	-/-/-	5.2/0.8/-	-/-/-	-/-/-	0.8/1.3/0.2
	0.50	0.5/0.6/0.1	0.2/0.1/-	2.5/3.3/1.3	-/-/-	5.2/1.7/0.1	-/-/-	-/-/-	0.8/0.9/0.5
	0.90	-/-/-	0.1/0.1/-	0.2/2.2/1.7	-/-/-	6.3/2.3/0.2	-/-/-	-/-/-	0.3/1.1/0.4

The analysis of the particles Ø < 1 µm in steel C showed that the majority of fine particles were still Ti- and Nb-based: the frequency of these elements was 92–95%, and the mean chemical composition 40–43%. Examples are shown in Fig. 17.

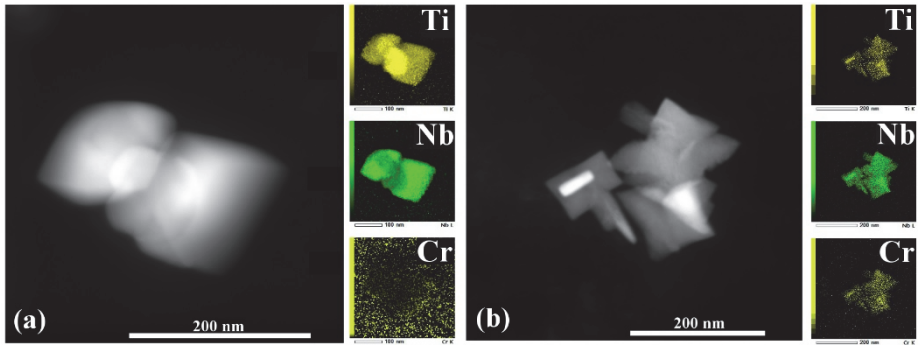

Fig. 17. STEM-EDS analyses of extracted particles in the low, 0.3 kJ/mm, heat input scenario of steel C: 54%Nb, 29%Ti, 11%Cu, others (Cr, Fe) <5% (a) and 52%Nb, 20%Cr, 17%Ti, others (Cu, Fe) <5% (b). [Paper V, reprinted by permission of Springer]

Based on statistical analyses, the best correlation between the DBTT and the measured parameters was seen with the grain size and the total number density of large TiN-rich and TiC-rich particles with ECD ≥ 2 µm. The regression model shown in Fig. 18 was compiled to describe the factors influencing DBTT. The model had R^2(adj.) = 0.80 and SE = 10 °C. The contribution of grain size to the variance was 58% and that of TiN and TiC-rich particles was 25%.

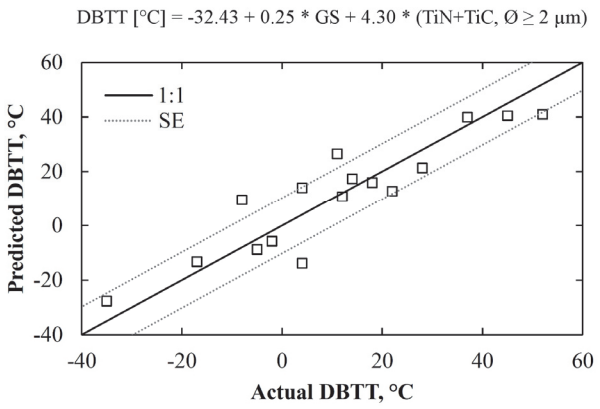

Fig. 18. Predicted vs. measured DBTT. In the regression model shown, GS denotes grain size in microns and (TiN+TiC, Ø ≥ 2 µm) the total number of TiN and TiC particles with ECD ≥ 2 µm per frame (frame size 27600 µm^2). [Paper V, modified and reprinted by permission of Springer]

4.4.4 Fracture appearance vs. impact toughness

The fracture surfaces were examined in Papers III–VI after impact toughness testing. Generally, ductile parts failed by microvoid coalescence and brittle parts by multifaceted transgranular cleavage. Microvoids frequently contained inclusions and precipitates, and large nitrides were easily distinguishable on the cleavage planes, as seen in Fig. 19. Despite extensive searching for cleavage crack nucleation sites near the notches of broken Charpy-V samples, only in a few cases could particles be identified as potential cleavage crack nuclei, seen in Fig. 20.

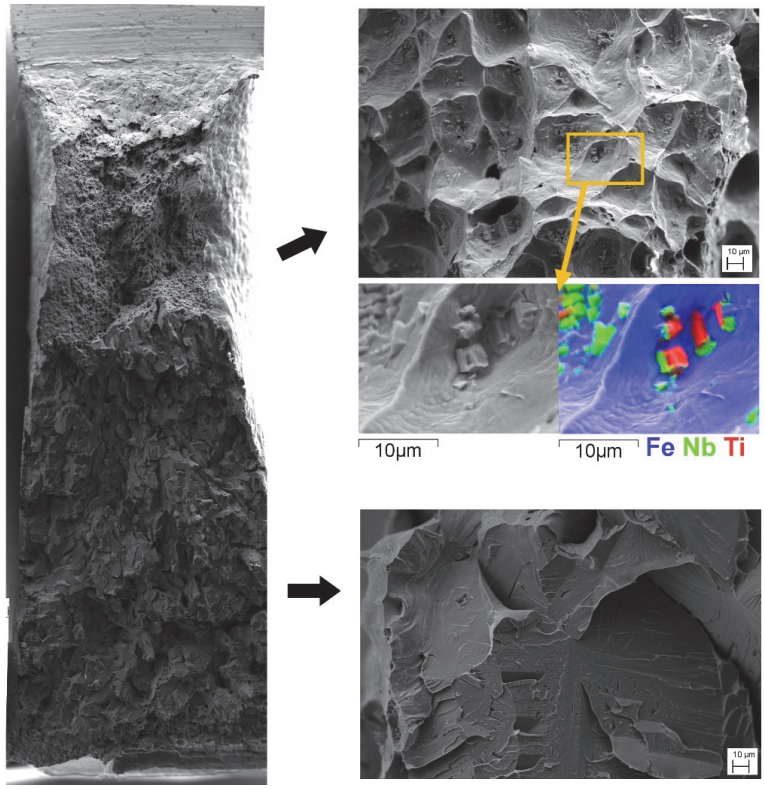

Fig. 19. Example of fracture surface: ductile fracture (top) and brittle fracture (bottom). The specimen had impact energy of 127 J/cm^2 and 30% of ductile fracture. [Paper IV, reprinted by permission of ASMET]

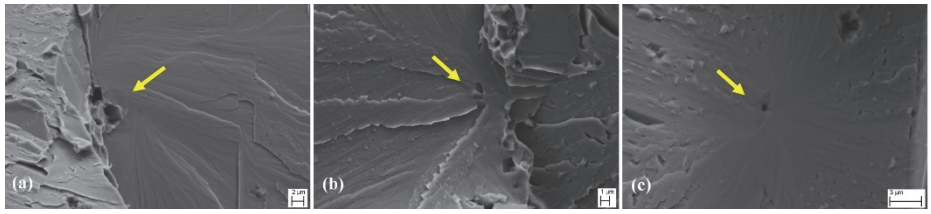

Fig. 20. Potential cleavage fracture initiation sites: grain boundary TiN (a), intragranular TiN (b), intragranular Ti-rich particle (c). [Paper V, modified and reprinted by permission of Springer]

Paper IV further correlated the measured impact energy to the amount of ductile fracture seen at the surface of broken Charpy-V specimens. Interestingly, in many

instances, the 35 J/cm^2 transition temperature criterion was reached even with essentially brittle specimens with ductile fracture ≤ 10% on the whole fractured surface. A good fit was seen between the fracture appearance and absorbed impact energy normalized to the upper shelf energy, seen in Fig. 21a. Even stronger correlation was obtained when the essentially martensitic HAZ and weld metals of grade 1.4003 were excluded from the data, seen in Fig. 21b.

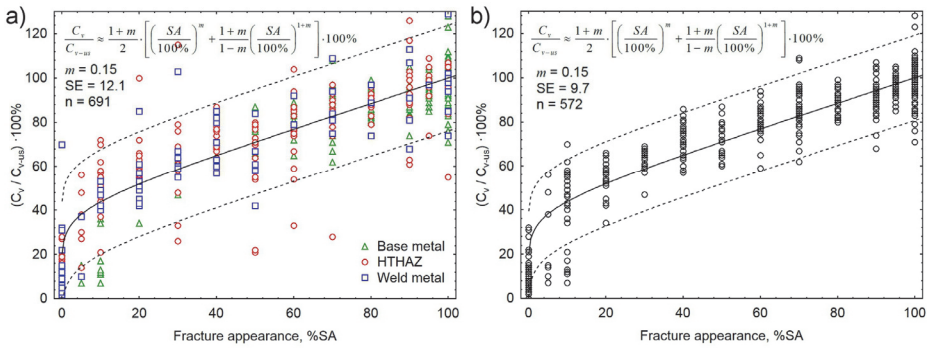

Fig. 21. The relationship between normalized impact energy ($C_v/C_{v\text{-}us}$) and fracture appearance (%SA) in 1.5–6 mm ferritic stainless steels. All specimens (a), excluding the martensitic specimens of grade 1.4003 (b). [Paper IV, modified and reprinted by permission of ASMET]

5 Discussion

In medium- and high-Cr ferritic stainless steels, the stabilized grades generally offer improved mechanical and corrosion properties over those of the unstabilized grades. Superior properties are achieved with steels having very low interstitial contents of 100 mass ppm and below. The more commercially viable intermediate interstitial contents of 200–500 mass ppm offer limited improvements. Moreover, the alloying requirements to stabilize intermediate purity steels can cause issues in the production, e.g. nozzle clogging and surface inclusion issues.

5.1 Influence of minor elements on the weldability issues of stabilized ferritic stainless steels

In this study, the use of various steelmaking and stabilization practices was shown to influence the weldability of intermediate purity stabilized ferritic stainless steels. The main contributing elements that were found to have an effect were Al, Ca, Si, Ti and Nb.

5.1.1 Aluminium

The Al used in deoxidation, in combination with Ti originating from the stabilization, was shown to promote glassy slag island films that could cover the entire front part of the weld pool. These slags could maintain their stability and occasionally travel on top of the weld pool through the weld cycle. Slag lumps and films have been observed and examined in various steels, often as a secondary topic in weld penetration and arc interaction studies. Fifty years ago, Linnert [110] noted that, in addition to globular slag islands, very light unidentified oxide films can appear and cover GTA weld pools. Chase and Savage [132] used high-purity Ni alloy with various chemical additives in stationary GTA welds and hypothesized that certain additions, such as Al and Ti, could alter the weld pool characteristics by forming solids floating on the surface of the weld pool. Metcalfe and Quigley [133] described that Al, V, Mo and Ti were seen in stainless steel welding slags in much higher concentrations than in the bulk. The authors infrequently saw slag islands floating around the weld pool but also a thinner scum that was easily moved by the surface currents on the weld pool. However, a detailed characterization of these surface contaminants was not completed, but they were shown to contain higher levels of Al and Ti than the bulk. Espinosa [134] observed Al particles and

film at the outer regions of the HY-80 steel GTA weld pool. Lambert [135] described two types of slag in Alloy 800 after welding; a film that covered almost the entire weld pool and other slag spots that were at the edges of the pool. Mills et al. [136] described continuous films rich in Ca (80%) in stainless steel welds with only smaller amounts of Al, Cr and Fe oxides (< 20%).

It is postulated that various terms in the literature used to describe slag islands (slag spots, white spots, black spots, silicate islands, scum, rafts, films, patches, refractory oxides) make it difficult to separate slag types from each other. The literature generally supports the existence of films, but the term 'film' is used inconsistently. As was evidenced in video imaging, the thin film could travel with the weld pool throughout the welding and could easily be unnoticed if slagging was judged only by the naked eye after welding. Nevertheless, the Al-bearing Ti-containing films of this study most accurately resemble pure alumina patch-type slags that Pollard [106] identified after welding in austenitic stainless steels. The author suggests that these slags are solid in the outer parts and liquid in the inner parts of the weld pool.

The temperature in the GTA weld pool surface is typically in the range of 1600–2100 °C, depending on the welding parameters used [104, 106, 108, 109, 136]. The stability of the film in this study was found to be related to the concentration of Al but also to the arc current, i.e., in Paper I, the tendency to form ignition slags seen after welding diminished as the current increased from 75 A to 125 A. Even though the chemistry of the film would be expected to change with the Al/Ti ratio in the bulk, the mean composition of the film was measured to be 42 wt.% Al – 15 wt.% Ti, the remainder being oxygen. These findings could be explained with reasonable accuracy with the aid of equilibrium thermodynamic calculations, the results of which are shown in Fig. 22. The figure shows that the solubility of the oxides in the molten steel increases as the temperature increases and the amount of the Al-bearing corundum phase in the system decreases. The figure also shows that as the Al content in the system decreases, the temperature range where the corundum phase is stable becomes smaller. Naturally, these considerations neglect the turbulence and steep temperature gradients in the weld pool that may cause additional interactions.

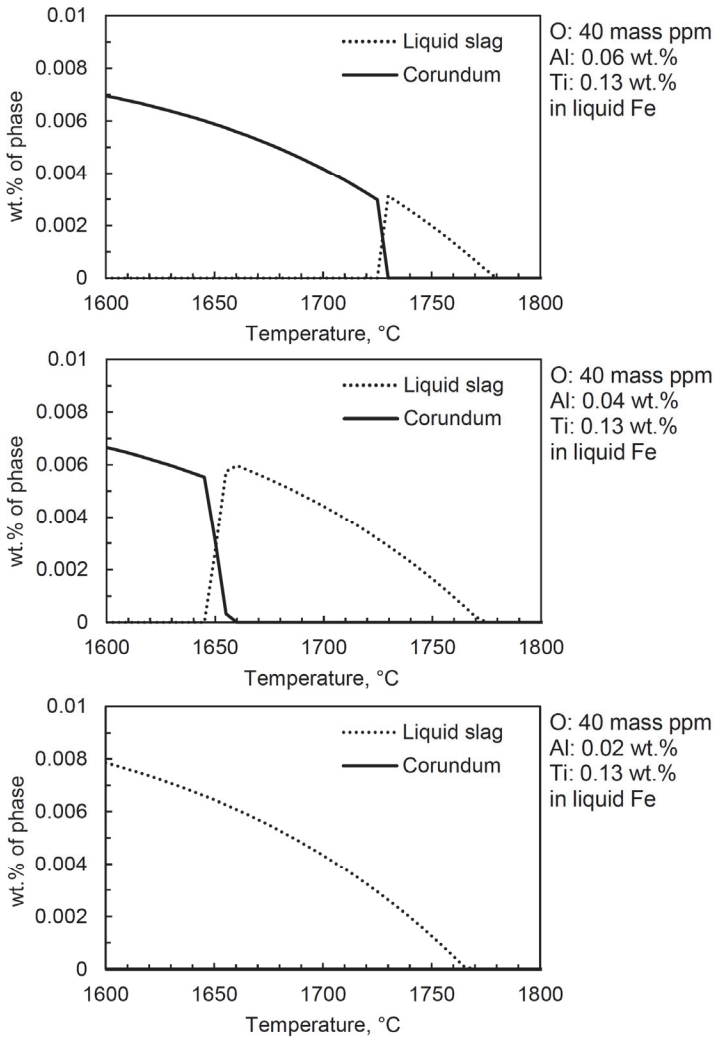

Fig. 22. Al- and Ti-bearing oxide phases at equilibrium in liquid Fe in the system Fe-0.13Ti-0.0040O and varying Al concentrations in the range of 0.02–0.06 wt.%. (Liquid slag: 48–84% TiO_2 and/or Ti_2O_3, 15–51% Al_2O_3; Corundum: 97–98% Al_2O_3). Calculated using Fact-Sage 7.1 thermodynamic equilibrium database.

Pollard [106] found that Al-rich slag patches caused an irregular weld penetration profile. Mills et al. [136] and Mills and Keene [137] summarized that any films that may exist in the weld pool reduce the velocity of thermocapillary-driven fluid flow and may lead to stagnant zones in the weld pool. Consequently, differences between

inward and outward fluid flow would diminish. Also, they hypothesized that slag at the rear of the weld pool would, eventually, as it grows, attract the arc and cause irregularities in the fluid flow. In this study, a changing penetration profile was seen in some of the welds in Paper I, but no simple correlation was found between slagging and weld penetration. Based on the findings of Paper II, the subtle and changing nature of the glassy Al-Ti films may lead to an irregular penetration profile.

5.1.2 Calcium

Ca used in inclusion shape control and calcium treatment used in steelmaking was statistically shown to affect both slagging intensity and weld penetration in Papers I and II. After oxygen, Ca was the most frequent element in slag islands and influenced two different slagging mechanisms. In combination with Al and Ti, it was shown to promote the formation of black slag island spots that were not responsible for the majority of the slag islands present after welding but did cause smaller local weld discontinuities. Also, in combination with Ti, it was the main contributor in the formation of the large slag spots seen at the rear of the weld pool. Owing to its high reactivity, Ca has been found frequently on slag islands [106, 111, 113, 136].

Due to their complexity, the Ca-bearing slag islands of this study are best understood with the aid of the equilibrium thermodynamic calculations presented in Fig. 23. When the data from visual slagging intensity (presented earlier in Table 6) is compared with the calculated amount of slag at equilibrium in liquid Fe, it is seen that an increase in Ca concentration increases the stability and amount of slags. In practice, the calculations propose that in high-Ca steels, there is a wider temperature range for slags to form, and this is seen as an increase in the slagging intensity. The details of the situation in an actual weld pool will no doubt differ from the equilibrium states shown in the figure, but the trends with respect to temperature and Ca concentration can at least be expected to be valid.

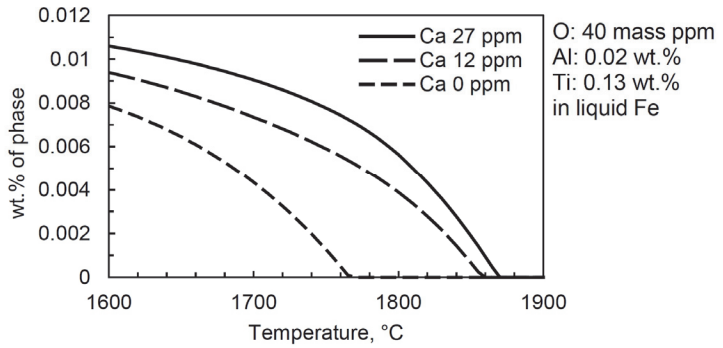

Fig. 23. Total amount of solid and liquid slags at equilibrium in liquid Fe in the system Fe-0.13Ti-0.02Al-0.0040O with varying Ca concentrations in the range of 0–27 mass ppm. Calculated using Fact-Sage 7.1 thermodynamic equilibrium database.

On a weight-% basis, Ca was also seen to have the largest negative effect on weld penetration. The harmful effect of Ca on weld penetration has been reported by various researchers. They attribute this either to the formation of CaS and CaO, which reduces the free S and O that should promote inward fluid flow, or to the formation of slag islands that disturb the fluid flow [136, 138, 139]. In this study, the likely effect of Ca was the entrapment of S and O as the Ca-rich slag islands had little effect on the weld penetration level. These observations are analogous to Pollard [106] who found that globular slag spots had little effect on weld penetration.

5.1.3 Silicon

Surprisingly, Si was not found to be a major element in slag islands, as none of the analysed slag islands contained Si above the 5 wt.% threshold limit. Pollard [106] emphasized that Si/Al ratio in the bulk would explain the slag island type, i.e., patch-type slags would form when this ratio was below 50, and globular-type slags would form above. In this study, there was no evidence to support this conclusion, probably due to the presence of the other more stable oxide formers Ca and Ti. However, in the present study, Si was shown to deteriorate weld penetration to a similar magnitude as Ca, when the minimum–maximum ranges of the elements are considered. This effect can be explained in two ways: Si can reduce the available O by forming relatively unstable oxides (compared to those of Al, Ca and Ti), but perhaps more importantly, Si is known to decrease the viscosity (increase the

fluidity) of the melt. Therefore, the outward fluid flow characteristic of low S steels could be more pronounced with high Si content, analogous to the early findings of Oyler et al. [140].

5.1.4 Titanium

Based on the research in this work, the effects of Ti are all-encompassing in stabilized ferritic stainless steel welds. Titanium is present in all slag island mechanisms that were described in detail previously. Most notably, in low-Al, Ca-containing steels, the predominant slag islands will be Ca- and Ti-based and seen at the rear of the weld pool. When Ti is used for stabilization, its concentration is typically much higher compared with Al and Ca. Therefore, Ti readily reacts with oxygen, if given the opportunity. The presence of Ti in slag islands has been demonstrated by various authors [112, 113, 133].

In addition to slag islands, Ti was also shown to have a negative effect on weld penetration. The literature dealing with the effect of Ti on weld penetration is inconsistent [108]. However, in this study, the effects are best explained with the entrapment of O.

Furthermore, Ti was found to be beneficial in promoting grain refinement in the GMA welds of Paper III. The effect was expected based on the literature, as Ti nitrides and oxides can nucleate ferrite grains, given that those form at the molten weld pool ahead of the solidifying front [118, 141–143]. Conversely, it was also seen in Paper VI that relatively small amounts of Ti (700–800 mass ppm) in intermediate purity (170–210 mass ppm N) steels were insufficient to refine the grain structure in autogenous GTA welds. When the welds were doped with O and N via the shielding gas, grain refinement was probably achieved due to the enhanced stability of Al and Ti oxides and Ti nitrides, provided that N desorption was prevented. These findings conform by and large to the studies by Inui et al. [144, 145], who developed custom GMA welding wires to promote grain refinement. The authors propose a composition of 0.08 wt.% Ti, 0.04 wt.% Al and 0.1 wt.% N for optimal grain refinement and that the O content be about 300 ppm. Both proposals were achieved in this work with a shielding gas mixture that contained 1 vol.% O_2 and > 2 vol.% N_2, and significant grain refinement was achieved.

The influence of grain refinement on the toughness of the weld metal was complex. In Paper III, welds fabricated with the 430Ti filler wire generally showed improved toughness over coarse columnar-grained welds fabricated using 430LNb,

despite having a higher total interstitial content. The C content in the 430Ti filler wire was 700 mass ppm higher than in 430LNb, whereas there was only 90 mass ppm difference in N. However, the O and N doped fine-grained autogenous welds in Paper VI were more brittle than coarse-columnar grained welds. These discrepancies can be explained at least partly with the results of Paper V that dealt with the toughness of the HAZ: the results from those experiments showed that in addition to grain size, large Ti-carbonitride particles ($Ø \geq 2$ μm) in high total number density had a detrimental influence on impact toughness DBTT. The deteriorating effects of TiN-rich particles on toughness are expected. In ferritic stainless steels, large TiN particles have been shown to initiate cleavage cracks and promote microcracking in 18Cr-2Mo steel [87, 146]. Ghosh et al. [147] described how even relatively small $Ø > 0.5$ μm TiN could initiate cleavage cracks in high-strength low-alloy (HSLA) steels. However, Du et al. [148] could not find any statistically significant correlation between DBTT and TiN particles in such steels.

It is assumed that the deteriorating effects of TiN-rich particles in the weld metals are analogous to the HAZ. Even though the work reported here provides no quantitative data in support of the idea, it seems that the main difference between weld metals and HAZs is that the large nitrides originating from the base plate dissolve in welding and thereby reduce the average particle size, i.e., lower the probability of initiating microcracks. Then, when the formation of Ti-nitrides is promoted via N brought by the shielding gas, the average particle size is probably increased. Therefore, the benefits of grain refinement could be lost with increase in the particle size.

5.1.5 Niobium

Although the examined steels frequently contained Nb in ample amounts due to the stabilization requirements, the effects of Nb on the main topics of this thesis were small. Nb did not play any role in the slag island developments, which is not a surprise owing to its low tendency to form oxides. However, in the weld metals the most striking feature of the solely Nb-stabilized welds was their tendency to form coarse-columnar grained welds, i.e., their inability to refine the grain structure to any degree. The poor toughness properties obtained with Nb-stabilized filler metals can be related to the large grain size that has poor ability to arrest propagating cleavage cracks.

However, the benefits of Nb became most apparent with the HAZ toughness. The use of Nb stabilization instead of Ti has been shown to improve impact

toughness in base metals [50, 146]. In this study, the absence of large particle clusters and the more effective grain boundary pinning likely provided by Nb-rich precipitates led to the lowest DBTT in the HAZ of the solely Nb-stabilized steels. Apparently, the absence of large particles made the crack initiation more difficult. Furthermore, this allowed better tolerance against variance in the heat input.

5.2 Other aspects

In addition to the main contributing elements presented above, the results pointed out several other notable aspects.

In Paper I, it is shown that, despite being the main surface-active elements in steels, S and O contents showed no statistically significant effect on weld penetration for the ranges studied. In particular, the S content of all heats was very low, the mean value being only 4 ppm. These low values were clearly insufficient to promote inward fluid flow in weld pools. The estimated mean soluble S was even lower, 2 ppm, due to the presence of Ca that readily forms very stable CaS.

Heat input had a positive effect on penetration in partial penetration and full penetration welds. It is known that changes in the welding parameters may increase the magnitude of the difference in penetration level between heats, as the higher power density will enlarge the temperature gradient [109]. This might be the reason why low-heat input welds (e.g. D125 scenario) showed no significant difference, while higher heat input welds (D75) showed a stronger difference in the level of penetration. Higher currents may also induce electromagnetic forces, but those are generally only relevant above about 250 A [109]. Lambert [135] found that low current, low welding speed conditions minimize cast-to-cast variations in butt welds. However, in the present study, the high current and high welding speed minimized the differences, but heat input per unit length was the lowest compared to other scenarios.

Small differences in the steel inclusion structures prior to welding did not influence slagging behaviour. The composition of slag islands correlated best with the bulk composition of the steel rather than its inclusion structure. This is analogous to Pollard [106], who considered that slag islands would not reflect the original inclusion structure but more or less the equilibrium corresponding to temperatures near the surface of the weld pool.

The detrimental influence of grain size on toughness was clearly demonstrated in Paper V, where the grain size contributed 58% to the variance of DBTT. Typically, in ferritic stainless steels, an increase of 1 ASTM number over the range from 0 to

6.5 (decrease in grain size from 360 to 38 μm) lowers the DBTT by 6–26 degrees [13, 44, 149]. However, if this is achieved through a higher interstitial content, the beneficial effect is reduced due to precipitation [13, 16, 51, 149]. In this study, an increase of 1 ASTM number reduced the DBTT by 7–8 degrees over the range of 1.5 to 8.5 (210 to 19 μm), which is in line with these general observations.

Grain boundary precipitates promoted by slow cooling are also considered detrimental to the toughness of ultra-pure and intermediate purity ferritic stainless steels [13, 51]. However, in this study, the effect was either small or masked by stabilization. As an example, steel D in Table 9 did not show a significant increase in DBTT with low and medium heat inputs compared with unaffected base metal, despite the increase in grain size and grain boundary precipitation that surrounded basically every grain.

5.3 Practical implications

The research results of this study provide and verify several practical implications in the welding of intermediate purity stabilized ferritic stainless steels.

In alloy design, to minimize slagging tendency, maximize weld penetration and prevent other potential irregularities from occurring during welding, excessive Al deoxidation and Ca treatment should be avoided. This will prevent the accumulation of slag islands and potential problems associated with the formation of films. Simultaneously, if Si and Ti are kept at a low level, the weld penetration should improve. To minimize the grain growth and maximize the toughness in the HAZ, the stabilization should be entirely carried out by using Nb instead of Ti or mixed Ti+Nb stabilization. On the other hand, when the amount of Ti is low, the weld metal microstructure is prone to the formation of coarse columnar grains originating from the partially melted HAZ grains. Coarse-grained welds are more susceptible to brittle cleavage crack propagation. Also, grain impingement at the centreline of the weld may reduce the cracking resistance due to low melting point segregates. So, the best practice would be to stabilize steels predominantly with Nb and moderate the Ti and N contents to reduce the size of particles forming from the interdendritic liquid.

Regarding the selection of ferritic filler metals, the limited availability of ferritic filler metals may lead to instances when the recommended PWHT, for example to heal the potential sensitization, may reduce the toughness due to secondary phase embrittlement seen as Laves phases in Paper III. Also, the PWHTs that were carried out in this study appeared to shift the rupture in cross-weld tensile

tests to the weld metal, which is generally not favoured or not permitted in material specifications.

Benchmarking of the examined stabilized ferritic stainless steels position these materials in between the utility ferritic steel 1.4003 and traditional 1.4016 after welding. Generally, when the sheet thickness is above 3 mm, the impact toughness DBTTs in the weldments are at room temperature. It should also be kept in mind that the 35 J/cm^2 DBTT criterion does not mean that specimens having higher value than this would be fully ductile, quite the contrary. Moreover, if a more conservative approach would be used, e.g. a 50% ductile fracture transition criterion, the transition temperatures would frequently be above room temperature.

5.4 Reliability and limitations

In Paper I, the slagging intensity was judged visually, therefore, it is subjective, despite the criteria that were set. However, the elements that emerged from the regression analyses were analogous to the main elements found with EDS, i.e., Ca, Ti and Al. Therefore, it can be postulated that the visual observations were accurate. Similarly, in Papers IV and V, the fractions of ductile fracture in broken Charpy-V specimens were determined visually. The operator error in Paper IV was estimated by conducting a separate viewing session with another author. Specimens selected at random yielded a mean standard deviation of 5% between the authors in the transition range (specimens with 10–90% ductility), so the results can be considered relatively trustworthy.

Regression models that were presented regarding slagging (Papers I and II) and DBTT (Paper V) were assumed to be linear. The use of more complex models with interaction terms or nonlinearities could describe the phenomena with better accuracy. In Paper V, the standard error of the DBTT regression was 10 °C, which meets the recommendation of Wallin [150], that under no circumstances the scatter of the Charpy data should be estimated to be less than 10 °C.

When studying the characteristics of slag islands, inclusions and precipitates in EDS, it was necessary to remove the matrix contribution from the spectra. The normalized EDS analyses in Papers I, II and V assumed that Fe always originated from the matrix. Therefore, any Fe-rich precipitates would not be analysed properly. The presence of large ($Ø \geq 1$ μm) Fe-rich precipitates or inclusions in stabilized ferritic stainless steels is unlikely due to other more readily forming compounds such as those of Al, Ca, Cr, Mg, Nb, Si and Ti.

In order to simulate HAZ microstructures, a Gleeble thermomechanical simulator was utilized. The microstructures obtained from the simulations may not entirely represent the situation in practical welds with analogous heat inputs. Mainly, the effects of temperature gradients (thermal pinning) are larger in practical welds [151]. To minimize the discrepancy that might exist with different temperature gradients, a constant free span distance (20 mm) was used with all specimens during thermal simulations.

In Paper V, a limited number of compound groups and criteria were used. It is supposed that the majority of oxide, nitride and carbide particles were included (Al_2O_3, TiO_2, TiN, NbN, TiC, NbC and $Cr_{23}C_6$), however, the effects of sulphides were not considered. Also, it was assumed that the volumetrically largest compounds in a particle would dominate cleavage nucleation, and particle morphologies were not taken into account. STEM analyses were limited to one steel in Paper V. This also meant that particles Ø < 1 μm were not included in the regression analyses due to a lack of quantitative data.

Video imaging equipment used to observe slag islands *in situ* was limited to about 20 frames per second and a resolution of 992 × 1040 pixels. Therefore, any finer details were unperceivable.

When estimating the weld metal microstructures in Paper III, any pick-up reactions or element loss during welding was not considered.

5.5 Future work

The current study indicates that the topics listed below would require further investigations.

Due to low sheet thickness, the current range in the welding experiments of Papers I and II were limited to 60–140A, that may not present the situation in high current scenarios. Also, the slagging tendency was evaluated after single-pass welding scenarios. It would be wise to examine the slagging tendency in multi-pass welding; possibly with slags removed from the first-pass using pickling or grinding procedures.

The materials used in Papers I and II had very low S contents. Slagging mechanisms and characteristics taking place in high S, i.e., inward fluid flow, steels might be different to those seen in this study. Also, slagging studies were carried out only with dual-stabilized steel 1.4509, i.e., the investigated steels always contained an abundance of Ti. Further examinations should also consider ferritic stainless steels with other stabilizing elements.

The lengths of the practical welds were approximately 200 mm in Papers I and II. Therefore, any slagging characteristics that may change in longer welding runs were not revealed. For industrial purposes, especially relating to steels having low slagging tendency, it would be viable to carry out much longer welding tests, e.g. tens of meters, where the slag accumulation and interaction with the weld pool could be seen better corresponding to automatic welding lines.

Changes in the welding arc properties other than spectroscopic studies were outside the scope of this work. Slag islands have been reported to attract the welding arc, especially in low-S steels, where the outward fluid flow can propel the slags to the sides of the weld pool and cause irregularities in the welds. Visual and video imaging in this study did not reveal any clear arc wandering. However, further investigations to clarify the interplay of slag islands and welding arc should be carried out.

Only one reducing shielding gas variant (Ar+3%H_2) was used in the investigations regarding the avoidance of slagging in Paper II. Therefore, it would be necessary to carry out a more comprehensive study about the influence of reducing shielding gas on slagging intensity. Also, the use of H in shielding gas can run the risk of hydrogen embrittlement in ferritic stainless steel welds. Therefore, the study should also examine the mechanical properties, especially ductility and formability, of the welded joints.

In Paper II, the slagging imaging was carried out with a CCD camera and 20 fps acquisition rate. A high-speed, high-resolution camera would be the next step to investigating and verifying *in situ* slagging mechanisms.

The spectroscopy set-up used in Paper II acquired the spectra from the whole plasma that hindered the observation of the vaporization of elements near the surface of the weld pool. A device resembling that of Mills [152] that could separate the plasma regions would be necessary to investigate slagging interactions with the welding arc. Also, the slagging chemical analyses were limited to weld deposits. Analysis of welding electrode deposits similar to Lambert [135] may bring additional information about the vaporization of elements.

In Paper III, the low-Cr-stabilized steel 1.4512 was only welded using the comparable 409LNb filler metal. It would be reasonable to assess the feasibility of 430Ti and 430LNb filler metals with this steel grade as well, as the typical approach would be to use potentially more expensive or metallurgically dissimilar austenitic filler metals.

To continue the research presented in Paper V, more compound groups should be introduced so that the effect of sulphides, for example, could be taken into

account. Also, it would be important to include different particle morphologies that may have influence on microcracking and cleavage nucleation.

All toughness testing in this thesis was carried out using conventional Charpy-V impact testing. Instrumented impact toughness testing would bring quantitative information about the nature of the fracture during loading. More importantly, correlation of impact toughness to fracture toughness in differently stabilized ferritic stainless steel base metals and HAZs should be investigated.

Due to tarnishing of the GTA welding electrode, the grain refinement examinations that were carried out in Paper VI should be continued using other autogenous welding techniques such as double-shielded GTA, CO_2 or YAG laser welding.

6 Summary and conclusions

The influence of minor elements, especially Al, Ca, Si, Ti, Nb, N and O, on weldability were investigated in various intermediate purity stabilized ferritic stainless steels. The investigations focused on the influence of minor elements on the fluid flow of the weld pool, slag island developments, weld penetration, weld metal, HAZ microstructures and properties in a variety of welding processes and welding scenarios. Practical welding tests were complemented with Gleeble HAZ simulations. The aim of the study was to provide an up-to-date understanding regarding some of the issues in the weldability of modern stabilized ferritic stainless steels. The study also benchmarked the performance of commercial ferritic stainless steels and filler metals. A wide variety of techniques were utilized to characterize the materials: LOM, LCF, SEM, STEM, video imaging, welding parameter monitoring, *in situ* optical emission spectroscopy. Mechanical properties were evaluated using hardness, tensile, impact toughness, cracking resistance and formability tests. Some corrosion properties were evaluated with intergranular and oxidation tests. The main results and conclusions can be summarized as follows:

- Slag islands of two characteristics can be distinguished after welding: globular slag spots and slag patches associated with arc ignition. However, there can be at least three different slagging mechanisms that can take place in the weld pool simultaneously during welding: black spot developments, accumulation of slag at the rear of the weld pool and surface films. Slagging can be estimated from the bulk steel composition rather than the inclusion structure. The abundancy of Al used in deoxidation and extent of Ca treatment have the largest influence, but welding parameters also have some influence.
- Although Ca was the most predominant in controlling the weld penetration, given the ranges of Ti and Si seen in different 1.4509 heats, they are as important in controlling the weld penetration in low-S stabilized ferritic stainless steels. No statistical significance was seen with the surface-active elements S or O.
- No simple correlation existed between slag islands and weld penetration. However, Ca and Ti were found to be important in both. Also, inconsistencies in the behaviour of Al lead to the conclusion that the changing weld penetration might be linked to surface films that momentarily influence the transient fluid flow of the weld pool.

- Coarse columnar grains normally dominate the microstructure in GTA, GMA and laser welds, if the stabilization is mostly Nb-based. Titanium in combination with Al is needed to refine the grain structure. Significant grain refinement can be obtained in autogenous welding when the concentrations of N and O in the molten weld pool are raised by adding 1–10 vol.% N_2 and 0.5–3 vol.% O_2 via the shielding gas. These promote the stability of oxides and nitrides that eventually nucleate ferrite grains ahead of the solidification front extending from the partially melted HAZ grains. However, the effects can be unsuccessful, if the absorption of N_2 is not achieved.
- Coarse columnar-grained welds do not impair the tensile properties or ductility of the weldments. However, a reduction in impact toughness and cracking resistance was evident. Still, the refinement of the grain structure does not improve toughness, if it is accompanied with an increase in the interstitial content.
- In the base metals and coarse-grained HAZs, the best toughness is obtained with steels that have low Ti content. The grain size and carbonitride particle clusters $Ø \geq 2$ µm rich in Ti were statistically shown to govern the DBTT. Large TiN-rich particles are practically unaffected by the welding heat input in the HAZ and act as nuclei for cleavage cracks. Conversely, stabilization with Nb usually results in a finer grain size and prevents large particle clusters in the base metal and HAZ. Other particle clusters or grain boundary precipitates were relatively harmless.
- Absorbed impact energy alone is uninformative to characterize the fracture micro mechanisms taking place. Specimens that meet the 35 J/cm^2 criterion show no more than 10% of ductile fracture, which is a modest value. The 50% ductile fracture transition temperature is always more conservative.
- Improper PWHTs, such as those carried out at 750 °C for steel 1.4509, may promote secondary Laves phase formation and a reduction in impact toughness.

7 Novel features

To the best of the author's knowledge, the following findings are original to this work:

- Three slagging mechanisms can simultaneously exist in the weld pools of Ti-bearing stabilized ferritic stainless steels.
- Black spots developed from the elements Ca, Al and Ti in the steel being welded and caused weld discontinuities and disturbance to fluid flow.
- Surface films developed from Al deoxidation and Ti originating from the stabilization. Ca did not influence this mechanism. The film can easily go unnoticed when welds are examined after the welding process, and it is more unstable with higher welding currents. Large films affected the transient fluid flow of the weld pool, potentially affecting the weld penetration profile. However, no simple correlation was seen with post-welding slag islands and weld penetration.
- Slag accumulating at the rear of the weld pool was typical and most intense in steels with low Al, high Ca and Ti originating from the stabilization. A detachment of a large slag spot would often leave a residue that facilitated the development of large new spots instead of smaller spots.
- In low-S steels, Ca is not solely responsible for poor weld penetration, Si and Ti also impair weld penetration in stabilized ferritic stainless steels.
- Grain refinement is possible to achieve in autogenous welds that are prone to the formation of columnar grains, if the steel contains sufficient Ti and Al, and the weld pool is doped with N and O from the shielding gas. A wide slag is beneficial for the effect to take place, as it prevents N desorption.
- The grain size and carbonitride particle clusters rich in Ti with an ECD 2 µm or more control the DBTT in 21 wt.% stabilized intermediate purity ferritic stainless steels.

List of references

1. Cortie MB (1993) History and development of ferritic stainless steels. J South African Inst Min Metall 93:165–176
2. Appolloni L, Rocchi C, Guerra R, et al (2011) New grades of stabilized superferritic stainless steel: main properties and applications. In: 7th European Stainless Steel Conference Science and Market. AIM, Como, Italy: paper 13
3. Charles J, Mithieux J-D, Santacreu P-O, Peguet L (2009) The ferritic stainless family: the appropriate answer to nickel volatility? Rev Métallurgie 106:124–139
4. Thielsch H (1951) Physical and welding metallurgy of chromium stainless steels. Weld J 30:209s–250s
5. International Stainless Steel Forum (2017) Stainless steel in figures 2017
6. JFE Steel Co. (2011) JFE443CT, Technical data sheet
7. Acciai Speciali Terni (2013) 460LI - 21Cr, Technical data sheet
8. Acciai Speciali Terni (2013) 470LI - 24Cr, Technical data sheet
9. Outokumpu Stainless (2013) EN 1.4622, Technical data sheet
10. Aperam Stainless Europe (2012) K45, Technical data sheet
11. European Standardization Organization (2014) EN-ISO 10088-1
12. Lippold JC (1990) A review of the welding metallurgy and weldability of ferritic stainless steels. EWI, Ohio, USA
13. Wright RN (1980) Toughness of Ferritic Stainless Steels. In: Lula RA (ed) Toughness of ferritic stainless steels - ASTM Special Tech Publ. ASTM, West Conshohocken, PA, USA: 2–33
14. Kah DH, Dickinson DW (1981) Weldability of Ferritic Stainless Steels. Weld J 60:135s–142s
15. Binder WO, Spendelow HR (1951) The influence of chromium on the mechanical properties of plain chromium steels. Trans ASM 43:759–772
16. Krysiak KF (1986) Welding behaviour of ferritic stainless steels - An overview. Weld J 65:37–41
17. Plumtree A, Gullberg R (1980) Influence of interstitial and some substitutional alloying elements. In: Lula RA (ed) Toughness of ferritic stainless steels - ASTM Special Tech Publ. ASTM, West Conshohocken, PA, USA: 34–55
18. Kaltenhauser RH (1971) Improving the engineering properties of ferritic stainless steels. Met Eng Q 11:41–47
19. Lula R (1980) Introduction. In: Lula R (ed) Toughness of ferritic stainless steels - ASTM Special Tech Publ. ASTM, West Conshohocken, PA, USA: 1
20. Fisher RM, Dulis EJ, Carroll KG (1953) Identification of the precipitate accompanying 885°F embrittlement in chromium steels. J Met 197:690–695
21. Williams RO, Paxton HW (1957) The nature of ageing of binary iron-chromium alloys around 500°C. J Iron Steel Inst 185:358–374
22. Demo JJ (1977) Structure, constitution, and general characteristics of wrought ferritic stainless steels. ASTM, Philadelphia, USA

23. Nichol TJ, Datta A, Aggen G (1980) Embrittlement of ferritic stainless steels. Metall Trans A 11:573–585
24. Ohashi N, Ono Y, Kinoshita N, Yoshioka K (1980) Effects of metallurgical and mechanical factors on Charpy impact toughness of extra-low interstitial ferritic stainless steels. In: Lula R (ed) Toughness of ferritic stainless steels - ASTM Special Tech Publ. ASTM, West Conshohocken, PA, USA: 202–220
25. Brown EL, Burnett ME, Purtscher PT, Krauss G (1983) Intermetallic phase formation in 25Cr-3Mo-4Ni ferritic stainless steel. Metall Trans A 14:791–800
26. Sedriks AJ (1996) Corrosion of stainless steels, 2nd ed. Wiley, New York, USA
27. Lula RA (1976) Ferritic stainless steels: Corrosion resistance + economy. Met Prog 110:24–29
28. Nehrenberg AE, Lillys P (1954) High temperature transformations in ferritic stainless steels containing 17 to 25% chromium. Trans Am Soc Met 46:1177–1213
29. Castro R, Tricot R (1964) Study of the isothermal transformations in 17% Cr stainless steels, part II: Influence of carbon and nitrogen. Met Treat Drop Forg 31:469
30. Bond AP (1969) Mechanisms of intergranular corrosion in ferritic stainless steels. Trans Metall Soc AIME 245:2127–2134
31. Davison RM, Steigerwald RF (1979) The new ferritic stainless steels. Met Prog 116:40–46
32. Tverberg JC, Janikowski DS (2005) The Performance of superferritic stainless steels in high chloride waters. Stainl. Steel World 17:56–63
33. Kovach CW, Redmerski LS, Kurtz HD (1980) Crevice corrosion performance of a ferritic stainless steel designed for saline water condenser and heat exchanger applications. In: NACE - Corrosion 80, Chicago, USA: paper 95
34. Janikowski DS (2005) Super-ferritic stainless steels rediscovered. Stainl. Steel World 184–190
35. Yamamoto S, Kobayashi Y, Katahira M, et al (1988) High toughness, corrosion resistant ferritic stainless steel: High purity 18Cr-2Mo alloy. Nippon Kokan Tech Rep 52:17–24
36. Ishii K, Ishii T, Furukimi O (2006) US8465604B2 - Ferritic stainless steel sheet having excellent corrosion resistance and method of manufacturing the same
37. Chassagne F, Santacreu P (2007) EP20070290039 - Ferritic stainless steel with 19% of chromium stabilised with niobium
38. Ruffini F, Appolloni L, Brascugli G, et al (2009) WO2010016014A1 - Ferritic stainless steel
39. Calinski C, Strehblow H-H (1989) ISS depth profiles of the passive layer on Fe/Cr alloys. J Electrochem Soc 136:1328–1331
40. Hsieh C-C, Wu W (2012) Overview of intermetallic sigma phase precipitation in stainless steels. ISRN Metall 2012:1–16
41. Olsson C-OA, Landolt D (2003) Passive films on stainless steels—chemistry, structure and growth. Electrochim Acta 48:1093–1104
42. Kerber SJ, Tverberg JC (2000) Stainless steel surface analysis. Adv Mater Process 33–36

43. Hanawa T, Hiromoto S, Yamamoto A, et al (2002) XPS characterization of the surface oxide film of 316L stainless steel samples that were located in quasi-biological environments: Biomaterials and bioengineering. Mater Trans 43:3088–3092
44. Semchyshen M, Bond AP, Dundas H (1971) Effects of composition on ductility and toughness of ferritic stainless steels. In: Proceedings of the Symposium Toward Improved Ductility and Toughness. Kyoto, Japan: 239–253
45. Juuti TJ, Karjalainen LP, Rovatti L, et al (2011) Contribution of Mo and Si to Laves-phase precipitation in type 444 steel and its effect on steel properties. In: 7th European Stainless Steel Conference. Como, Italy: paper 77
46. Ujiro T, Satoh S, Staehle RW, Smyrl WH (2001) Effect of alloying Cu on the corrosion resistance of stainless steels in chloride media. Corros Sci 43:2185–2200
47. Yazawa Y, Yoshioka K, Togashi F (1994) Effects of Cr, Mo and Cu on the atmospheric corrosion resistance of ferritic stainless steels in a coastal environment. Kawasaki Steel Tech Rep 31:35–43
48. Shu J, Bi H, Li X, Xu Z (2012) The effect of copper and molybdenum on pitting corrosion and stress corrosion cracking behavior of ultra-pure ferritic stainless steels. Corros Sci 57:89–98
49. Abo H, Nakazawa T, Takemura S, et al (1977) The role of carbon and nitrogen on the toughness and intergranular corrosion of ferritic stainless steels. In: Stainless Steel ’77. London, UK: 35–47
50. Redmond J (1980) Toughness of 18Cr-2Mo stainless steel. In: Lula R (ed) Toughness of ferritic stainless steels - ASTM Special Tech Publ. ASTM, West Conshohocken, PA, USA: 123–144
51. Van Zwieten ACTM, Bulloch JH (1993) The influence of interstitial solute level on the Charpy toughness properties of a 40% Cr-Fe stainless steel. Int J Press Vessel Pip 56:69–91
52. Grubb J, Wright R, Farrar P, Jr (1980) Micromechanisms of brittle fracture in titanium-stabilized and alpha’-embrittled ferritic stainless steels. In: Lula R (ed) Toughness of ferritic stainless steels - ASTM Special Tech Publ. ASTM, West Conshohocken, PA, USA: 56–76
53. Gordon W, van Bennekom A (1996) Review of stabilisation of ferritic stainless steels. Mater. Sci. Technol. 12:126–131
54. Wood J (1980) Effect of residual elements and molybdenum additions on annealed and welded mechanical properties of 18Cr ferritic stainless steels. In: Lula RA (ed) Toughness of ferritic stainless steels - ASTM Special Tech Publ. ASTM, West Conshohocken, PA, USA: 145–160
55. Krysiak KF, Grubb JF, Pollard B, Campbell RD (1993) Selection of wrought ferritic stainless steels. In: ASM Handbook: Volume 6: Welding, Brazing, and Soldering, 10th ed. ASM International: 1299
56. Cowling RD, Hintermann HE (1971) The anodic oxidation of titanium carbide. J Electrochem Soc 118:1912–1916

57. Nichol TJ, Davis JA (1978) Intergranular corrosion testing and sensitization of two high-chromium ferritic stainless steels. In: Steigerwald RF (ed) Intergranual Corrosion of Stainless Alloys - ASTM Special Tech Publ. ASTM International: 179–196
58. Barteri M, Fortunati S, Sassetti L, et al (1987) Role of secondary phase precipitation in intergranular corrosion of differently stabilized ELI ferritic stainless steels. The Institute of Metals, York: 432–442
59. Creamer E (1980) 885°F embrittlement in 12Cr steel distillation column tray. In: Lula R (ed) Toughness of ferritic stainless steels - ASTM Special Tech Publ. ASTM, West Conshohocken, PA, USA: 291–296
60. Dong WB, Ma L, Jiang LZ (2007) Effects of Ti and Nb stabilization on the recrystallization and the pitting potential in Fe-21% Cr ferritic stainless steels. In: Materials Science Forum. Trans Tech Publ 561:77–80
61. Campbell RD (1987) An investigation into the physical metallurgy, welding metallurgy, hot-cracking and weld pool shape of ferritic stainless steels. Rensselaer Polytechnic Institute, Troy, NY, USA
62. Yushchenko KA, Morozova RI, Kakhovskii YN, Nastenko GF (1994) Effect of welding heat on embrittlement of chromium steels stabilised with titanium or niobium. Pat Weld J 6:380–383
63. Sello MP, Stumpf WE (2010) Laves phase embrittlement of the ferritic stainless steel type AISI 441. Mater Sci Eng A 527:5194–5202
64. Kato Y, Ito M, Kato Y, Furukimi O (2010) Effect of Si on precipitation behavior of Nb-Laves phase and amount of Nb in solid solution at elevated temperature in high purity 17% Cr-0.5% Nb steels. Mater Trans 51:1531–1535
65. Nakao Y, Nishimoto K, Noi S, et al (1987) The effect of zirconium on the bending ductility of the overlay welds of low interstitial ferritic stainless steels. Trans Japan Weld Soc 18:3–11
66. Rosenberger G, Wright R (1980) Toughness and fabrication response of Fecralloy strip. In: Lula R (ed) Toughness of ferritic stainless steels - ASTM Special Tech Publ. ASTM, West Conshohocken, PA, USA: 297–312
67. Sipos DJ, Steigerwald RF, Whitcomb NE (1972) US 3672876 - Ductile corrosion-resistant ferrous alloys containing chromium
68. Demo JJ (1976) US3992198 - Ductile chromium-containing ferritic alloys
69. Hio K, Tsutsui M, Hosoi Y (1999) Electrochemical characteristics of chromium-saving ferritic stainless steel. Corrosion 55:822–824
70. Cotterell KL (1986) The fracture toughness of high chromium ferritic stainless steel strip. Rensselaer Polytechnic Institute, Troy, NY, USA
71. Grobner PJ (1973) The 885 °F (475 °C) embrittlement of ferritic stainless steels. Metall Trans 4:251–260
72. Chih-Chun H, Weite W (2012) Overview of intermetallic sigma phase precipitation in stainless steels. ISRN Metall
73. Yamagishi T, Akita M, Nakajima M, et al (2010) Effect of σ-phase embrittlement on fatigue behaviour in high-chromium ferritic stainless steel. Procedia Eng 2:275–281

74. Guimarães AA, Mei PR (2004) Precipitation of carbides and sigma phase in AISI type 446 stainless steel under working conditions. J Mater Process Technol 155:1681–1689
75. Sawatani T, Minamino S, Morikawa H (1982) Effect of Laves phase on the properties of Ti and Nb stabilized low C, N-19% Cr-2% Mo stainless steel sheets. Trans Iron Steel Inst Japan 22:172–180
76. de Andrade TF, Kliauga AM, Plaut RL, Padilha AF (2008) Precipitation of Laves phase in a 28%Cr–4%Ni–2%Mo–Nb superferritic stainless steel. Mater Charact 59:503–507
77. Kobayashi S, Takeda T, Nakai K, et al (2011) Effect of Nb addition on Cu precipitation in ferritic stainless steel. ISIJ Int 51:657–662
78. Yan H, Bi H, Li X, Xu Z (2009) Precipitation and mechanical properties of Nb-modified ferritic stainless steel during isothermal aging. Mater Charact 60:204–209
79. Juuti TJ, Karjalainen LP, Heikkinen E-P (2012) Precipitation of Si and its influence on mechanical properties of type 441 stainless steel. Adv Mater Res 409:690–695
80. Han K, Hong S, Lee C (2012) The effect of the precipitates type on the thermal fatigue properties of 18% Cr ferritic stainless steel weld HAZ. Mater Sci Eng A 546:97–102
81. Kim SM, Chun YS, Won SY, et al (2013) Hydrogen embrittlement behavior of 430 and 445NF ferritic stainless steels. Metall Mater Trans A 44:1331–1339
82. Santacreu P-O, Faivre L, Acher A, Leseux J (2011) K44X: A new ferritic stainless steel grade with improved durability for high temperature exhaust manifolds. SAE Tech Pap No 2011-01-0194. SAE International
83. Moller GE, Franson IA, Nichol TJ (1980) Experience with ferritic stainless steel in petroleum refinery heat exchangers. In: Corrosion/80 NACE meeting. Chicago, USA: paper 53
84. Campbell RD (1992) Ferritic stainless steel welding metallurgy. Key Eng Mater 69:167–216
85. Ochiai SI, Saito N, Kikuta Y (1980) Effects of nitrogen and carbon on mechanical properties of weld-simulated 19% chromium steels. Trans Japan Weld Soc 11:129–135
86. Gooch TG, Ginn BJ (1990) Heat-affected zone toughness of MMA welded 12% Cr martensitic-ferritic steels. TWI Weld Inst Members Rep 3
87. Li Y, Zhang Y, Sun B, Wang J (2002) TEM observation and fracture morphology in the CGHAZ of a new 0Cr18Mo2Ti ferritic stainless steel. Bull Mater Sci 25:361–366
88. van Niekerk CJ, du Toit M, Erwee MW (2012) Sensitization of AISI 409 ferritic stainless steel during low heat input arc welding. Weld World 56:54–64
89. Lippold JC, Kotecki DJ (2005) Welding metallurgy and weldability of stainless steels. Wiley, Hoboken, NJ, USA
90. Demo JJ (1971) Mechanism of high temperature embrittlement and loss of corrosion resistance in AISI type 446 stainless steel. Corrosion 27:531–544
91. Nichol TJ, Franson IA, Moller GE (1982) Applications of new high chromium ferritic stainless steels in the chemical process industries. In: Corrosion/81. NACE: paper 117
92. Chawla SL, Gupta RK (1993) Materials selection for corrosion control. ASM International
93. Gulyaev AP, Levanova AN (1978) Brittleness of high-chromium ferritic stainless steels. Met Sci Heat Treat 20:881–886

94. Demo JJ (1974) Weldable and corrosion-resistant ferritic stainless steels. Metall Trans 5:2253–2256
95. Ikawa H, Nakao Y, Nishimoto K (1980) Embrittlement in the weld metal of high purity 30Cr-2Mo steel. Trans Japan Weld Soc 11:31–35
96. Botti CA (2006) Lean substitution options for 300 series alloys and commercially pure titanium. In: Stainless Steel World 2006 Conference. Houston, TX, USA
97. Deverell HE (1980) Toughness properties of vacuum induction melted high-chromium ferritic stainless steels. In: Lula RA (ed) Toughness of ferritic stainless steels - ASTM Special Tech Publ. ASTM, West Conshohocken, PA, USA: 184–201
98. Krysiak K (1980) Weldability of the new generation of ferritic stainless steels - update. In: Lula R (ed) Toughness of ferritic stainless steels - ASTM Special Tech Publ. ASTM, West Conshohocken, PA, USA: 221–240
99. Honeycombe J, Gooch TG (1983) Corrosion and stress corrosion of arc welds in 18% chromium–2% molybdenum–titanium stabilised stainless steel. Br Corros J 18:25–34
100. Honeycombe J, Gooch TG (1981) Mechanical properties of arc welds in 18% chromium 2% molybdenum titanium stabilised ferritic stainless steel. In: Proc. Second Joint Welding Convention 'Integrity of Welding'. AWI, NZIW, Christchurch, New Zealand
101. Scribner L (1980) Evaluation of high-purity 26Cr-1Mo ferritic stainless steel welds by burst tests. In: Lula R (ed) Toughness of ferritic stainless steels - ASTM Special Tech Publ. ASTM, West Conshohocken, PA, USA: 241–254
102. Mills KC, Keene BJ, Brooks RF, Shirali A (1998) Marangoni effects in welding. Philos. Trans. R. Soc. A Math. Phys. Eng. Sci. 356:911–925
103. Heiple C, Roper J, Stagner R, Aden R (1983) Surface active element effects on the shape of GTA, laser and electron beam welds. Weld J 72–77
104. Modenesi PJ (2015) The chemistry of TIG weld bead formation. Weld Int 29:1–12
105. Heiple CR, Roper JR (1982) Mechanism for minor element effect on GTA fusion zone geometry. Weld J 61:97s–102s
106. Pollard B (1988) The effects of minor elements on the welding characteristics of stainless steel. Weld J 67:202s–213s
107. Ryan MP, Williams DE, Chater RJ, et al (2002) Why stainless steel corrodes. Nature 415:770–774
108. Mills KC, Keene BJ (1990) Factors affecting variable weld penetration. Int Mater Rev 35:185–216
109. Burgardt P, Heiple C (1986) Interaction between impurities and welding variables in determining GTA weld shape. Weld J 150–155
110. Linnert G (1967) Weldabílity of austenitic stainless steels as affected by residual elements. In: Effects of residual elements on properties of austenitic stainless steels. ASTM International: 105–119
111. Harvey MDF, Rodwell MH (1988) The influence of TIG welding procedure on slag island formation on a Type 316 stainless steel - a case study. TWI Ind Memb Rep Summ 358/1988

112. Collins S (1997) Stainless steel for semiconductor applications. In: Mechanical working and steel processing conference. Warrendale, PA, USA: 607–619
113. Rau J (2003) The effect of trace elements on the formation of slag spots during gas tungsten arc welding of 316 L stainless steel tube systems. SEMI Stainless Steel Task Force Meeting. San Francisco, CA, USA: 1–7
114. Matsuhashi T, Nakata M (2013) US20130129560A1 - Ferritic stainless steel
115. Nelson TW, Lippold JC, Mills MJ (1999) Nature and evolution of the fusion boundary in ferritic-austenitic dissimilar weld metals, Part 1-Nucleation and growth. Weld J 78:329s
116. Kou S (2003) Welding metallurgy. John Wiley & Sons, Hoboken, NJ, USA
117. Kou S, Le Y (1982) The effect of quenching on the solidification structure and transformation behavior of stainless steel welds. Metall Mater Trans A 13:1141–1152
118. Villafuerte JC, Kerr HW, David SA (1995) Mechanisms of equiaxed grain formation in ferritic stainless steel gas tungsten arc welds. Mater Sci Eng A 194:187–191
119. Davies GJ, Garland JG (1975) Solidification structures and properties of fusion welds. Int Metall Rev 20:83–108
120. Directorate-General for Research and Innovation (European Commission) (2011) Grain size control in steel by means of dispersed non-metallic inclusions – GRAINCONT. Final report. RFCS publications, Brussels, Belgium
121. Kimura K, Takahashi A (2010) Development of NSSC{®} PDX—a ferritic stainless steel with excellent formability. Nippon Steel Tech Rep 99:51–55
122. Thomas C, Apps R (1980) Weld heat-affected zone properties in AISI 409 ferritic stainless steel. In: Lula R (ed) Toughness of ferritic stainless steels - ASTM Special Tech Publ. ASTM, West Conshohocken, PA, USA: 161–183
123. Vigor C (1980) Effect of cold-working on impact transition temperature of 409 and E-4 stainless steels. In: Lula R (ed) Toughness of ferritic stainless steels - ASTM Special Tech Publ. ASTM, West Conshohocken, PA, USA: 255–272
124. Eckenrod J, Kovach C (1980) Development of a low-chromium stainless steel for structural application. In: Lula R (ed) Toughness of ferritic stainless steels - ASTM Special Tech Publ. ASTM, West Conshohocken, PA, USA: 273–290
125. Mintz B, Arrowsmith J (1980) Impact properties of Fe-13Cr thick plate. In: Lula R (ed) Toughness of ferritic stainless steels - ASTM Special Tech Publ. ASTM, West Conshohocken, PA, USA: 313–335
126. Thomas C, Apps R (1984) A study into the structure and properties of the heat-affected zone in 18Cr2Mo ferritic stainless steels. In: Lula RA (ed) New Developments in Stainless Steel Technology. ASM International: 351–379
127. Thomas CR, Robinson FPA (1978) Kinetics and mechanism of grain growth during welding in niobium-stabilized 17% chromium stainless steels. Met Technol 5:133–138
128. Humphreys FJ, Hatherly M (2004) Recrystallization and related annealing phenomena, 2nd ed. Elsevier, Kidlington, Oxford, UK
129. Anttila S, Heikkinen H-P, Lantto S, Säynäjäkangas J (2013) Weldability evaluation of five ferritic stainless steels for structural purposes. In: Proceedings of the 17th International Conference on Joining Materials (JOM-17). Helsingør, Denmark

130. Nakazawa T, Suzuki S, Sunami T, Sogo Y (1980) Application of high-purity ferritic stainless steel plates to welded structures. In: Lula R (ed) Toughness of ferritic stainless steels - ASTM Special Tech Publ. ASTM, West Conshohocken, PA, USA: 99–122
131. Espy RH (1982) Weldability of nitrogen-strengthened stainless steels. Weld J 43:149–156
132. Chase TF, Savage WF (1971) Effect of anode composition on tungsten arc characteristics. Weld J 50:467–473
133. Metcalfe JC, Quigley MBC (1977) Arc and pool instability in GTA welding. Weld J 56:133–139
134. Espinosa DC (1991) Visualisation of gas tungsten arc weld pools. Naval Postgraduate School. Monterey, CA, USA
135. Lambert J (1989) Welding procedure selection to minimise cast-to-cast variability in thin section TIG (tungsten inert gas) butt welds. In: CEGB Report RD/M/1784/RR89
136. Mills KC, Brooks RF, Shirali A (1992) The effect of low levels of calcium on weld penetration. Comm Eur Communities: 70
137. Mills KC, Keene BJ (1990) Factors affecting variable weld penetration. Int. Mater. Rev. 185–216
138. Leinonen JI, Järvenpää SA, Karjalainen LP (1992) Harmful effect of calcium on weld penetration characteristics. In: Intl. Conf. Trends in Welding Research. Gatlinburg, TN, USA: 712–717
139. Burgardt P, Campbell RD (1992) Chemistry effects on stainless steel weld penetration. Key Eng Mater 69–70:379
140. Oyler GE, Matuszesk RA, Carr RC (1967) Why some heats of stainless steel may not weld. Weld J 46:1006–1011
141. Madeira RP, Modenesi PJ (2010) The study of 430Ti and 430LNb ferritic welding wires for application in the cold part of automotive exhaust systems. Weld Int 24:412–421
142. Bayraktar E, Katundi D, Yilbas BS, Claeys J (2011) Toughness of welded stainless steels sheets for automotive industry. J Achiev Mater Manuf Eng 44:35–41
143. Villafuerte JC, Pardo E, Kerr HW (1990) The effect of alloy composition and welding conditions on columnar-equiaxed transitions in ferritic stainless steel gas-tungsten arc welds. Metall Mater Trans A 21:2009–2019
144. Inui K, Noda T, Shimizu T, Nagata M (2003) Development of the ferritic stainless steel welding wire providing fine grain microstructure weld metal for the components of automotive exhaust system. SAE Tech Pap 2003-01-0979. SAE International
145. Inui K, Minamikawa H, Noda T (2006) US7026576 - Welding wire and welding method using the wire
146. Han J, Li H, Xu H (2014) Microalloying effects on microstructure and mechanical properties of 18Cr-2Mo ferritic stainless steel heavy plates. Mater Des 58:518–526
147. Ghosh A, Ray A, Chakrabarti D, Davis CL (2013) Cleavage initiation in steel: Competition between large grains and large particles. Mater Sci Eng A 561:126–135
148. Du J, Strangwood M, Davis CL (2012) Effect of TiN particles and grain size on the Charpy impact transition temperature in steels. J Mater Sci Technol 28:878–888

149. Plumtree A, Gullberg R (1974) The influence of interstitial content on the ductile-brittle transition temperature of Fe-25Cr ferritic stainless steels. J Test Eval 2:331–335
150. Wallin K (2011) Fracture toughness of engineering materials: Estimation and application. EMAS Publishing. Warrington, UK
151. Alberry PJ, Chew B, Jones WKC (1977) Prior austenite grain growth in heat-affected zone of a 0.5Cr-Mo-V steel. Met Technol 4:317–325
152. Mills G (1977) Use of emission spectroscopy for welding arc analysis. Weld J 93–96

Original publications

I Anttila S, Lauhikari V, Heikkinen H-P & Porter D (2016) Slag island characteristics and weld penetration in very low sulphur 18% Cr stabilized ferritic stainless steel, Welding in the World 60(3): 485–496.

II Anttila S, Aula M & Porter D (2017) Behaviour and influence of slag islands in ferritic stainless steel welds, Welding in the World 61(6): 1141–1154.

III Anttila S, Karjalainen P & Lantto S (2013) Mechanical properties of ferritic stainless steel welds in using type 409 and 430 filler metals, Welding in the World 57(3): 335–347.

IV Anttila S, Heikkinen H-P, Säynäjäkangas J & Porter D (2015) Impact energy and fracture appearance in welds of some ferritic stainless steels, Proc 8th European Stainless Steel Conference, Austrian Society for Metallurgy and Materials (ASMET).

V Anttila S, Alatarvas T & Porter D (2017) Factors affecting impact toughness in stabilized intermediate purity 21Cr ferritic stainless steels and their simulated heat-affected zones, Metallurgical and Materials Transactions A 48(12): 5879–5889.

VI Anttila S & Porter D (2014) Influence of shielding gases on grain refinement in welds of stabilized 21%Cr ferritic stainless steel, Welding in the World 58(6): 805–817.

Reprinted with permission of Springer (I–III, V, VI) and the Austrian Society for Metallurgy and Materials (IV).

Original publications are not included in the electronic version of the dissertation.

653. Hajimammadov, Rashad (2018) Plasmonic, electrical and catalytic properties of one-dimensional copper nanowires : effect of native oxides

654. Barua, Bidushi (2018) Incentivizing user participation in cooperative content delivery for wireless networks

655. Pallaspuro, Sakari (2018) On the factors affecting the ductile-brittle transition in as-quenched fully and partially martensitic low-carbon steels

656. Kyösti, Pekka (2018) Radio channel modelling for 5G telecommunication system evaluation and over the air testing

657. Petäjäjärvi, Juha (2018) Low-power wireless communications in the Internet of Things : solutions and evaluations

658. Boulkenafet, Zinelabidine (2018) Face presentation attack detection using texture analysis

659. Kaikkonen, Harri (2018) Supporting rapid product development with agile development methodologies

660. Tervo, Oskari (2018) Transceiver optimization for energy-efficient multiantenna cellular networks

661. Menberu, Meseret Walle (2018) Hydrology of peat-dominated headwater catchments : theories and empirical analysis of the impacts of anthropogenic disturbance

662. Hietava, Anne (2018) Electrical behaviour of submerged arc furnace's charge materials

663. Lappalainen, K. Matti (2018) Itämeren rehevöitymisen uudistettu diagnoosi ja paradigma

664. Ahmad, Ijaz (2018) Improving software defined cognitive and secure networking

665. Laiyemo, Ayotunde Oluwaseun (2018) High speed moving networks in future wireless systems

666. Kaleva, Jarkko (2018) Decentralized multiantenna transceiver optimization for heterogeneous networks

667. Hänninen, Tuomo (2018) Detection algorithms and FPGA implementations for SC-FDMA uplink receivers

668. Huotari, Joni (2018) Vanadium oxide nanostructures and thin films for gas sensor applications

Book orders:
Granum: Virtual book store
http://granum.uta.fi/granum/

UNIVERSITY OF OULU P.O. Box 8000 FI-90014 UNIVERSITY OF OULU FINLAND

ACTA UNIVERSITATIS OULUENSIS

SERIES EDITORS

A
SCIENTIAE RERUM NATURALIUM
University Lecturer Tuomo Glumoff

B
HUMANIORA
University Lecturer Santeri Palviainen

C
TECHNICA
Postdoctoral research fellow Sanna Taskila

D
MEDICA
Professor Olli Vuolteenaho

E
SCIENTIAE RERUM SOCIALIUM
University Lecturer Veli-Matti Ulvinen

F
SCRIPTA ACADEMICA
Planning Director Pertti Tikkanen

G
OECONOMICA
Professor Jari Juga

H
ARCHITECTONICA
University Lecturer Anu Soikkeli

EDITOR IN CHIEF
Professor Olli Vuolteenaho

PUBLICATIONS EDITOR
Publications Editor Kirsti Nurkkala

UNIVERSITY of OULU
OULUN YLIOPISTO

ISBN 978-952-62-1972-1 (Paperback)
ISBN 978-952-62-1973-8 (PDF)
ISSN 0355-3213 (Print)
ISSN 1796-2226 (Online)